Naval Research Laboratory

DTIC FILE COPY

AD-A224 145

Numerical Simulations of Flowfields in a Central-Dump Ramjet Combustor
III. Effects of Chemistry

KAZHIKATHRA KAILASANATH, JOHN H. GARDNER,
JAY P. BORIS, AND ELAINE S. ORAN

Center for Reactive Flow and Dynamical Systems Branch
Laboratory for Computational Physics and Fluid Dynamics

July 23, 1990

DTIC
ELECTE
JUL 25 1990
S B D

REPORT DOCUMENTATION PAGE

Public reporting burden for this collection of information is estimated to average 1 hour per response, including the time for reviewing instructions, searching existing data sources, gathering and maintaining the data needed, and completing and reviewing the collection of information. Send comments regarding this burden estimate or any other aspect of this collection of information, including suggestions for reducing this burden, to Washington Headquarters Services, Directorate for Information Operations and Reports, 1215 Jefferson Davis Highway, Suite 1204, Arlington, VA 22202-4302, and to the Office of Management and Budget, Paperwork Reduction Project (0704-0188), Washington, DC 20503.

1. AGENCY USE ONLY (Leave blank)	2. REPORT DATE 1990 July 23	3. REPORT TYPE AND DATES COVERED Interim

4. TITLE AND SUBTITLE	5. FUNDING NUMBERS
Numerical Simulations of Flowfields in a Central-Dump Ramjet Combustor III. Effects of Chemistry	ONR

6. AUTHOR(S)

Kazhikathra Kailasanath, John H. Gardner
J. P. Boris, and Elaine S. Oran

7. PERFORMING ORGANIZATION NAME(S) AND ADDRESS(ES)	8. PERFORMING ORGANIZATION REPORT NUMBER
Naval Research Laboratory Washington, DC 20375-5000	NRL Memorandum Report 6682

9. SPONSORING/MONITORING AGENCY NAME(S) AND ADDRESS(ES)	10. SPONSORING/MONITORING AGENCY REPORT NUMBER
Office of Naval Research 800 N. Quincy Street Arlington, VA 22217-5999	

11. SUPPLEMENTARY NOTES

12a. DISTRIBUTION/AVAILABILITY STATEMENT	12b. DISTRIBUTION CODE
Approved for public release; distribution unlimited.	

13. ABSTRACT (Maximum 200 words)

This report is the third in a series which presents the results of numerical simulations performed to isolate and study acoustic-vortex-chemical interactions in an idealized ramjet consisting of an axisymmetric inlet and combustor and a choked nozzle. Both reactive and nonreactive flows have been simulated. The nonreactive flow calculations show complex interactions among the natural instability frequency of the shear layer at the inlet-combustor junction and the acoustics of both the inlet and the combustor. The entire flow oscillates at a low frequency which corresponds to that of a quarter-wave mode in the inlet. For the reactive flow cases studied, energy release alters the flow field substantially. Energy release in a large vortex is in phase with the pressure oscillation over a substantial region of the combustor and results in the observed amplification of the low-frequency oscillations and leads to combustion instability. The large pressure oscillation also modifies the vortex shedding process.) The simulations also show that pre-energy release chemistry does not play a dominant role in controlling combustion instabilities in the system considered.

14. SUBJECT TERMS		15. NUMBER OF PAGES 53
Ramjet, Turbulence Combustion Instability.		16. PRICE CODE

17. SECURITY CLASSIFICATION OF REPORT	18. SECURITY CLASSIFICATION OF THIS PAGE	19. SECURITY CLASSIFICATION OF ABSTRACT	20. LIMITATION OF ABSTRACT
UNCLASSIFIED	UNCLASSIFIED	UNCLASSIFIED	UL

CONTENTS

Accession For

NTIS GRA&I	✓
DTIC TAB	☐
Unannounced	☐
Justification	

By____

Distribution/

Availability Codes

| | Avail and/or |
| Dist | Special |

A-1

DTIC
COPY
INSPECTED
8

iii

NUMERICAL SIMULATIONS OF FLOWFIELDS IN A CENTRAL-DUMP RAMJET COMBUSTOR
III. EFFECTS OF CHEMISTRY

1. INTRODUCTION

This report is the third in a series which presents the results of numerical simulations performed to isolate and study the interaction between acoustic waves, large-scale vortex structures and chemical energy release in an idealized, central-dump ramjet combustor. The first report dealt primarily with tests of the model and the effects of acoustic forcing [1]. The second report focused on the effects of the inlet and combustor acoustics and discussed the extent to which acoustic waves can influence vortex-rollup and merging patterns in the confined geometry of a combustor[2]. In this report, we discuss the effects of chemical energy release on the flow field in the combustor.

The idealized ramjet consists of an axisymmetric inlet connected to a combustor of larger diameter and an exit nozzle. High-speed flows separate at the inlet-combustor junction and the separated shear layer is usually turbulent. Such transitional shear layers are characterized by large-scale vortical structures. The interactions among these vortical structures can generate acoustic waves. Furthermore, the interactions themselves can be affected by the acoustic waves in the system. Energy release can have a substantial influence on the acoustic-vortex interactions by modifying the acoustic waves in the system. The nonlinear interactions among acoustic waves, large-scale vortex structures and chemical energy release affects the efficient operation of the system and may even result in combustion instability.

In recent years, numerical simulations have been used to study the flow over rearward facing steps [see for e.g.3-5] and in axisymmetric centerbody [6] and dump combustors [7]. Although simulations of the flow over a rearward facing step in a combustor have some features similar to the problem discussed here, they are very different in one important factor that they ignore the effects of acoustics on the flow field [5]. In the numerical study of

1

a dump-combustor flow field [7], there was fair agreement between the computed quantities such as mean axial velocity profiles and experimental data. However, these computations predicted a steady solution with a large recirculation zone. Simulations of a centerbody combustor [6] showed an oscillating flow field with periodic vortex shedding. Neither of these simulations considered the effects of an exit nozzle or acoustic waves on the flow field in the combustor. More recent simulations have considered the effects of exit nozzles [8-10] and the acoustics of the inlet and combustor [8,10].

In an earlier paper [11], we discussed the effects of increasing the inflow Mach number on the nonreacting flow field in the same combustor simulated here. These calculations showed vortex shedding at either the natural instability frequency of the shear layer or the first longitudinal mode frequency of the combustor if that was close to the natural shedding frequency. In all cases, the vortex mergings within the combustor were significantly influenced by the acoustics of the ramjet. In some cases, a low-frequency pressure oscillation was observed. The entire flow in the combustor was also periodic at this low frequency. Other simulations [10,12] have shown that the acoustics of the inlet determines this low frequency. Preliminary calculations with chemical reactions showed that energy release does not substantially change the frequency of this oscillation [13]. Such low-frequency oscillations which depend on the acoustics of the inlet have been observed in experiments in dump combustors with a constricted exit [14].

In this paper, we first briefly discuss a nonreactive flow simulation in which a mixture of hydrogen and air with a mean velocity of 200 m/s flows into an axisymmetric combustor. In this simulation, the natural instability frequency of the shear layer is very different from the first longitudinal acoustic-mode frequency of the combustor. As expected, vortex shedding occurs at the natural instability frequency of the shear layer. The vortex merging process in the combustor is affected by the acoustics of both the inlet and the combustor. Then simulations are presented in which these same cold flow is ignited and there is energy release from chemical reactions. The details of the flow field are significantly altered by energy release resulting in very different vortex shedding and merging patterns. The

2

reasons for these changes in global features of the flow and for the observed increase in the amplitude of the pressure oscillations is examined in this paper. The effects of changing one of the chemical reaction times is also discussed.

2. THE NUMERICAL MODEL

The numerical model solves the compressible, time-dependent, conservation equations for mass, momentum and energy in a two-dimensional axisymmetric geometry. The fluid dynamics and chemistry terms in the conservation equations are solved separately and coupled using timestep splitting [15]. The algorithm used for fluid dynamic convection is Flux-Corrected Transport (FCT) [16], a conservative, monotonic algorithm with fourth-order phase accuracy. FCT algorithms can be constructed as a weighted average of a low-order and a high-order finite-difference scheme. During a convective transport timestep, FCT first modifies the linear properties of the high-order algorithm by adding diffusion. This prevents dispersive ripples from arising and ensures that all conserved quantities remain monotonic and positive. Then FCT subtracts out the added diffusion in regions away from discontinuities. Thus it maintains a high order of accuracy while enforcing positivity and monotonicity. With various initial and boundary conditions, this algorithm has been used previously to solve a wide variety of problems in both supersonic reacting flows [17-19] and subsonic turbulent shear flows [10,20,21].

The calculations presented below are inviscid, that is, no explicit term representing physical viscosity has been included in the model. Also, no artificial viscosity is needed to stabilize the algorithm. There is a residual numerical diffusion present which effectively behaves like a viscosity term for short-wavelength modes on the order of the zone size. Unlike most numerical methods, however, the damping of the short-wavelength modes is nonlinear. Thus the effects of this residual viscosity diminish very quickly for the long wavelength modes, which results in a high effective Reynolds number. In the problem considered in this paper, we are primarily interested in the interaction of the acoustic modes with large-scale vortex structures, which is essentially an inviscid interaction.

The calculations reported here are essentially large-eddy simulations which model the fluid instabilities leading to transition to turbulent flow although no explicit subgrid turbulence model is used. The nonlinear properties of the FCT algorithm maintain the large-scale structures without aliasing while numerically smoothing the scales with wave-
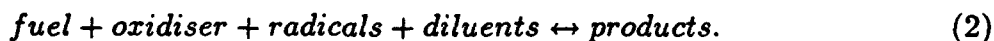
4

lengths smaller than a few computational cells. The question of how this high frequency filter acts is currently a topic of research.

The Reaction Model

The large number of species and reactions involved make it computationally impractical to include a detailed chemical reaction rate scheme in a complex multidimensional fluid dynamic problem such as the one discussed here. A detailed reaction rate scheme even for a 'simple' fuel such as hydrogen in air involves 9 species and about 50 reactions [22]. Therefore we have modelled the combustion of premixed hydrogen-air mixture using a simplified two-step parametric model. The first step is an induction step during which there is no energy release. The second step models the energy release process and starts only after the induction time has elapsed. During the induction step, the reactions taking place are modelled by

$$fuel + oxidiser + diluents \leftrightarrow radicals \tag{1}$$
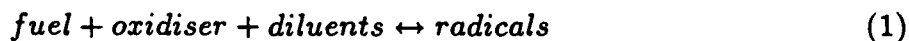
and during the energy release step,

$$fuel + oxidiser + radicals + diluents \leftrightarrow products. \tag{2}$$

In an actual combustion system both steps occur simultaneously after the first step has been initiated. However, during the induction step, the change in the concentrations and the amount of energy released are small enough that they can be neglected in a simplified model. Thus the temperature and pressure may be assumed to be constant during the induction period. This simplification enables us to use the chemical induction time data which are usually available at constant temperatures and pressures for mixtures of specified stoichiometry. The induction time data may be obtained from experiments or from calculations using detailed elementary reaction mechanisms[22]. We have used a table of induction times which were obtained by integrating a detailed set of reaction rates [23]. These induction times have been compared to experimental data where available and found to be in good agreement [22].

When combustion occurs in a fluid dynamic system, temperatures (and species concentrations) can change due to convective and diffusive transport processes. Here, convective mixing is assumed to be the dominant mechanism for bringing the premixed fuel-air mixture in contact with the hot, burnt products. Therefore, diffusive transport processes such as thermal conduction and molecular diffusion are not explicitly taken into account in the model. This is a reasonable assumption for the high-speed flow discussed in this paper because in most of the flow field, the characteristic times for the diffusive transport processes are much longer than the characteristic flow times (0.1 ms per cm). However, when the convective process brings the burnt and unburnt material in close proximity (within a few computational cells), diffusive processes may become important if the temperature and species gradients are large. Such length scales are not adequately resolved in the computations and hence over such length scales we consider mixing to take place within one computational time-step (which is of the order of 0.1 microseconds). This approach does lead to questions about how realistically the actual mixing process is modelled. Although such information is essential for a "complete" description of the problem, it is beyond current capabilities and furthermore does not significantly affect the results presented in this paper as discussed later.

To account for the fluid motion during the induction phase, we define an induction reaction progress variable I_{rp} that is convected with the fluid,

$$\frac{\partial(\rho I_{rp})}{\partial t} + \frac{\partial(\rho I_{rp}u)}{\partial x} + \frac{\partial(\rho I_{rp}v)}{\partial y} = \frac{\rho}{\tau_i(T, P, \phi)}. \tag{3}$$

The parameter I_{rp} integrates in a Lagrangian sense the time history of the temperature and pressure seen by a reacting fluid element as it is convected. Initially, I_{rp} is zero and when it reaches the value 1, the induction reaction ends and the energy release reaction begins.

In general, an energy release reaction step can be written as

$$\frac{d\rho_f}{dt} = -(\rho_f)^a(\rho_o)^b(\rho_p)^c A \exp\left(-E/RT\right) \tag{4}$$

6

where ρ_f is the concentration of the fuel, ρ_o is the concentration of the oxidiser, ρ_p is the concentration of the products, A is the pre-exponential factor and E is the activation energy, a, b, c depend on the order of the reaction given by equation (2). The parameters in equation (4) can be obtained either from fits to experimental data or by systematically reducing a multistep complex reaction mechanism to a fewer number of steps and in the limit to a single step. Both these processes are difficult because it is not possible in general to completely describe a complex chemically reactive system by a single step. However, certain global features of the chemistry may often be describable by simplified reaction mechanisms. There are many efforts currently underway to achieve simplified reaction models [eg. 24, 25]. It is risky to arbitrarily assign values for the various parameters because of the difficulty in assessing the sensitivity to a large set of parameters. Because of this uncertainity, we have chosen a particularly simplified model by assuming a to be 1, b and c to be zero and the activation energy to be small. This reduces equation (4) to

$$\frac{d\rho_f}{dt} = -A(\rho_f). \qquad (5)$$

An advantage to this approach is that it gives a simple expression for the characteristic time for energy release,

$$\tau_r = \frac{1}{A}. \qquad (6)$$

This allows us to easily vary τ_r to assess the coupling between energy release and fluid dynamics. Another approach to arriving at Equation (5) is to express the products and oxidiser densities in terms of the fuel density, so that the rate of reaction depends only on the fuel density. For the problem discussed in this paper, we have assumed $\tau_r = A^{-1} = 10 \ \mu$ s.

For completing the parametric model, the value of the final concentration of the fuel is also required. This can be obtained from equilibrium calculations or by assuming all the fuel is consumed for a fuel-lean case. Specification of the final concentration of the fuel determines the amount of energy released. We have chosen the final concentration

7

such that the burnt mixture temperature is 1400 K. The calculations presented below are therefore typical of a lean hydrogen-air mixture.

We have successfully used similar models in the past in one-dimensional and multi-dimensional reactive flow calculations [23, 26]. As a test of the validity of the reaction model, we compare the results of a one-dimensional shock tube problem obtained using the two-step parametric model to those obtained using a complete reaction mechanism for a dilute hydrogen-oxygen mixture. In Fig. 1a , the temperature is shown as a function of time and in Fig. 1b, the spatial distribution of temperature in the shock tube is shown at a particular time. Both figures show encouraging agreement in the overall features of the flow. The good agreement observed in the above test does not necessarily imply that the results obtained using the model in a complex multidimensional flow field such as in a combustor will be quantitative. The emphasis in this paper is on the qualitative effects of energy release on the flow field and the coupling between the energy released and the pressure field in the combustor. Future calculations will include varying the energy release times and the amount of energy release to gain a qualitative understanding of the effects of these parameters on the flow field in the combustor.

<u>Geometry and Boundary Conditions</u>

A schematic of the idealized central-dump combustor used in the simulations is shown in Fig. 2. A cylindrical jet with a prescribed mean velocity (200 m/s for the simulations descibed here) flows through an inlet of diameter, D into a cylindrical combustion chamber (dump combustor) of larger diameter. The dump combustor acts as an acoustic cavity and its length can be varied to change the frequency of the first longitudinal mode. An annular exit nozzle at the end of the chamber is modelled to produce choked flow.

The initial thrust of the modelling was to develop appropriate inflow and outflow boundary conditions [1,8]. The choked outflow conditions force the flow to become sonic at the throat of the exit nozzle. The choked outflow conditions force the flow to become sonic at the exit plane. In the code this is implemented by first calculating the critical conditions [27] (when sonic condition is attained) using the isentropic flow relations between

the physical properties in the last computational cell and the   'ane. Then, the density and energy are specified in a "guard" cell just outside the co.. putational domain, such that, the density and energy at the exit plane (which is the interface between the last cell and the guard cell) are the critical conditions. The flow velocity at the exit plane is also set to be sonic. These conditions are realistic because under most operating conditions in practical systems, the flow is choked at the throat of the exit nozzle. Furthermore, it has the computational advantage that the solutions are not affected by any numerical disturbances at the boundary. At solid walls the normal flux is set to zero and the pressure is extrapolated to the normal stagnation condition. No restriction is imposed on the tangential velocity near the walls. At the inflow, the pressure is allowed to fluctuate, but the mass flow rate and the inflow velocity are specified. These conditions allow the acoustic waves to reflect without amplification or damping at the inflow. These inflow boundary conditions could be modified to partially damp the acoustic waves originating downstream. More detailed discussions and tests of the boundary conditions have been presented in earlier papers [1, 10].

The computational cell spacing was held fixed in time. Fine zones were used near the entrance to the combustor (the dump plane) in both the radial and axial directions. In both directions the cell sizes gradually increased away from the dump plane. The effects of numerical resolution were checked by comparing calculations with 20×50, 40×100 and 80×200 cells. These grids were generated by either doubling or halving the cell sizes used in the 40×100 cell calculations. The 20×50 grid was too coarse to resolve the vortex shedding and merging resolved by the other two grids. With the finer 80×200 grid, smaller structures and higher frequencies can be resolved than with the coarser (40×100) grid. However, it was found that the 40×100 grid was adequate to resolve the major frequencies and all the large-scale structures observed in the cold flow [1, 10]. In order to improve the resolution of the flame front, a 60×120 grid is used in the calculations reported here. The smallest cell size in this grid is comparable to those in the 80×200 grid. The smallest cell size in the radial direction is 0.0529 cm and in the axial direction is

9

0.3069 cm. A typical timestep in the reactive flow calculations is 0.144 μs and takes 0.25 s of CPU time on the NRL CRAY X-MP/24 computer.

3. RESULTS AND DISCUSSION

The numerical simulations predict values of the density, momentum, and energy for each of the computational cells as a function of time. From this information we can selectively generate the various physical diagnostics. The analysis presented below uses three diagnostics extensively: the local time-dependent velocity and pressure fluctuations at various locations in the flow field, the time-dependent energy release at various stations in the combustor, and instantaneous flow visualization at selected times. For flow visualization, we use streamlines and temperature contours. Streamlines of the instantaneous flow field are a useful visual diagnostic for studying the structure of the flow. They also allow correlation and tracking of the coherent vortex structures and their merging patterns.

The physical dimensions of the inlet and combustor used in the simulations are given in Fig. 2. In addition, the exit consists of an annular ring at 0.633 D (from the axis of the combustor) with an area of 17.63 cm^2. The mass inflow rate is 0.95 kg/s with a mean velocity of 200 m/s. The inflowing gas is a premixed, lean hydrogen-air mixture at an initial temperature of 550 K.

The calculations were carried out to 160,000 timesteps without considering the effects of chemical reactions. Below we first discuss these "cold-flow simulations" and then present results of the reactive flow simulations.

Cold-Flow Simulations

Low-Frequency Oscillations

In some of our previous simulations [8,10,12], we observed a low-frequency oscillation which corresponded to the quarter-wave mode of the inlet. Furthermore, the entire flow field was periodic at this frequency. The relation between the low frequency pressure oscillation and the vortex merging patterns and its effect on the periodicity of the flow field has been discussed earlier [12]. With these previous results in mind, we first look at the acoustic mode in the inlet for this simulation.

The fourier analysis of the pressure fluctuations at various locations in the inlet is shown in Fig 3. The dominant frequency near the upstream end of the inlet (−8.21 D) is 250 Hz, the quarter-wave mode frequency of the inlet. As we move closer to the combustor, the amplitude of the 250 Hz mode decreases and the fluctuations at other frequencies become comparable. If the downstream end of the inlet behaved like an ideal open end, the amplitude at 250 Hz should decrease as we move towards it and reach zero at the dump plane. We see small amplitudes near the dump plane (−0.74 D) at 250 Hz and other frequencies due to interactions with the acoustics of the combustor and vortex shedding from the combustor-step.

Figure 4 shows a sequence of streamlines within the combustor at selected times. In each frame, the dump plane is at the left and the exit plane is at the right. The flow fields in all four frames are similar with five distinct large-scale structures at about the same locations in the combustor. The time interval between the first three frames is about 4 ms giving a frequency of 250 Hz. The third and fourth frames are about 3.56 ms apart giving a frequency of 280 Hz. This shift in the periodicity may be due to an increase in the acoustic frequencies or may be due to cycle to cycle variations. We also note that the first two frames are more like each other and so are the third and fourth frames. This again could be an indication of variations between different quasi-periodic patterns.

Vortex-Merging Frequencies

The fourier analyses of velocity fluctuations shown in Fig. 5 are at two locations in the combustor between which frequent vortex mergings are observed. The three dominant frequencies in the spectra at 4.21 D are 270, 530 and 770 Hz. Two of these frequencies are close to acoustic frequencies of the system. The quarter-wave mode frequency of the inlet is 250 Hz and the first longitudinal mode frequency is about 760 Hz. The dominant frequencies at 5.47 D are 530 Hz and 760 Hz. There are some fluctuations at 250 Hz also. Let us now look at what these frequencies correspond to in the flow field.

A series of snapshots of the flow field are shown in Fig. 6. The specific frames in this figure were chosen because they depict vortex mergings occuring between 4 and 5.5 D.

The time intervals between the various frames are not all same, suggesting that vortex mergings are not occuring with an unique frequency. The first two frames depict events that are 1.34 ms apart and this corresponds to a frequency of about 750 Hz. The time interval between the second and third frames is also 1.34 ms. However, the size and shape of the vortices taking part in the merging in frame three is different from that in the earlier frames. The time interval between this frame (third) and the next is only 0.89 ms. The next two frames(fourth and fifth) are again 1.34 ms apart. The time interval between the fifth and the sixth frames is quite different from the others and is 1.9 ms. This corresponds to a frequency of about 525 Hz. The sixth and seventh frames are only 0.78 ms apart. The seventh and the eighth frames are again 1.34 ms apart. Therefore we see that the vortex mergings are occuring primarily at about 750 Hz or the first longitudinal-mode frequency of the combustor. However, mergings are also occuring at 525 Hz and other frequencies higher than 750 Hz. The 525 Hz is probably a beat frequency between the dominant inlet and combustor frequencies. The exact origin of the higher frequencies is not clear. The presence of these frequencies results in small variations from cycle to cycle. These frequencies may be created because of a mismatch between the vortex shedding frequency and the dominant acoustic frequencies of the system.

Vortex Shedding and Merging near the Combustor Step

The fourier analyses of velocity fluctuations at two locations close to the step in the combustor are shown in Fig. 7. At 0.07 D from the dump plane, there is only one dominant frequency, 2810 Hz. This is probably the "natural" vortex-shedding frequency of the shear layer at the combustor step. At 0.98 D, there are at least four significant frequencies, 2810, 1310, 1510 and 3020 Hz. The frequencies of 1510 and 3020 Hz correspond to the second and fourth longitudinal acoustic-mode frequencies of the combustor. The other frequency, 1310 Hz, is probably a vortex-merging frequency.

A series of snapshots of the flow field at a constant interval of 0.11 ms or 500 timesteps is shown in Fig. 8. New vortices appear near the combustor step in the first, fourth and seventh frames. That is, vortex shedding occurs approximately every 1500 timesteps.

This corresponds to a frequency of about 3000 Hz. It is difficult to determine the vortex shedding frequency precisely from contour plots such as in Fig. 8 where the flow field is depicted only every 0.11 ms. Based on the fourier analysis of the velocity fluctuations at 0.07 D and the flow field visualization, we conclude that vortex shedding occurs with a frequency of about 2800 Hz.

For a configuration such as the one discussed in this paper, it is difficult to define a characteristic thickness for the shear layer at the combustor step because of the large recirculation zone. The momentum thickness is highly dependent on the velocity cut-off chosen. Because viscosity is not explicitly included in these simulations, the smallest scale in these calculations is the grid spacing in the transverse direction at the combustor step. However, a necessary condition for the shear layer to go unstable is an inflection point in the velocity profile. In order to resolve an inflection point, at least two computational cells are required. Therefore we take the width of two cells as a characteristic dimension for the shear layer thickness. In this simulation, this thickness is 0.106 cm. Using this thickness and a frequency of 2800 Hz, we obtain a Strouhal number of 0.015. An initially laminar shear layer has been observed experimentally [28] to roll up at $St_\theta = 0.012$. The theoretical value [29] is 0.017. Considering the uncertainity in the determination of the shear layer thickness in our simulations, the value of 0.015 for the Strouhal number suggests that the frequency of about 2800 Hz is the natural instability frequency of the shear layer in the simulations.

The paths of the vortices have also been drawn in Fig. 8. They show that the vortex shed at timestep 101,500 merges with the one shed at timestep 100,000 around timestep 103,500. The merging location is within one diameter of the step in the combustor. The previous timestep at which such a merging occurred is 100,000. Therefore the approximate merging frequency at this location is 1400 Hz. Figure 8 also shows the two processes by which vortices grow: entrainment of the surrounding fluid and vortex merging. The vortex shed at timestep 100,000 grows by entraining the surrounding fluid before another vortex merges with it.

14

The frequencies of 3020 and 1510 Hz are acoustic frequencies of the system. They probably appear because of the vortex shedding and merging that occur at frequencies close to them and they might in turn affect the vortical processes. Ocassionally, vortex shedding and mergings might be occurring at these acoustic frequencies. This process may be the cause of the observed cycle to cycle variations. It is difficult to categorically separate the acoustic fields from the solenoidal fields.

Effects of Energy Release

The mixture was ignited at timestep 160000 by assuming that the induction time has elapsed for a pocket of the gaseous mixture near the step. This causes the mixture to begin releasing its energy. The instantaneous flow fields in the combustor are shown at a sequence of timesteps in Fig. 9 using two different visualizations, contours of constant temperature and streamlines. Although timestep 160000 is before any energy release has occured, there are temperature fluctuations due to the compressibility of the flow. At step 165000, energy release has caused a reaction front (flamefront) distinguished by the location of the high-temperature contours and the darkened lines caused by closely spaced contours. The presence of a vortex near the step at this time is seen in Fig. 9b and the entrainement of the cold gases by it can be seen in Fig. 9a. With time, the shear layer roll-up causes the reaction front to curve downwards and engulf the cold mixture which subsequently burns. As the reaction front moves downstream, a new vortex forms near the step between timesteps 175000 and 180000. This mixes the burnt gases with the incoming fuel-air mixture and acts as an ignition source. Except for the first time at step 160000, it was not necessary to provide an external ignition source. The relation between the flamefronts and the vortices in the subsequent frames can be established by comparing the two figures. Comparing the flow fields at steps 160000 and 165000, one can see how rapidly energy release alters the features of the cold flow.

Another interesting observation from Fig. 9a is the presence of an unburned gas pocket at step 185000. This pocket of material has been cut off by the interaction of two flamefronts, seen at step 180000. The pocket subsequently burns up and its remnants can be

seen in the center of the forward most (closer to the exit) structure in step 190000. By step 195000, the flamefronts have reached the rear wall of the combustor and the burnt material has begun to exit.

Streamlines and temperature contours depicting the flow field in the combustor at a subsequent sequence of timesteps are shown in Figs. 10a and b. The presence of large-scale vortex structures in the reactive flow case is evident from these figures. The flow fields at steps 200000 and 225000 and those at 205000 and 230000 are similar to each other, suggesting that the reactive flow field undergoes a cycle of roughly 25000 timesteps or 3.463 ms. This corresponds to a frequency of 288 Hz, which is close to the low frequency of about 250-280 Hz observed in the cold-flow simulations. The pressure and velocity fluctuation spectra at all locations are dominated by this low frequency.

The drastic effect of energy release on the vortical flowfield can be seen in Fig. 11 where streamlines are used to compare the cold flow to the reactive flow over one cycle of the low frequency oscillation. In general, the effect of energy release is to form fewer and larger-scale vortices. The flowfields at steps 200000 and 225000 show that a large-scale vortex rollup occurs at the low frequency of about 288 Hz. However, vortex shedding does occur more frequently as seen in steps 205000 and 215000. These small vortices merge quickly to the larger vortex generated periodically at 288 Hz resulting in a still larger vortex which dominates the entire flow field. As discussed below, energy release in this large vortex is crucial in amplifying the low frequency oscillation.

<u>Unsteady Energy Release</u>

Figures 9 and 10 indicate that combustion is associated with vortices in the flow field. This can result in both temporal and spatial variations in the energy released. The total energy released in the entire combustor, shown as a function of time in Fig. 12, indicates that energy release is oscillatory. The amount of energy released and the peaks of the oscillations increase with time. These increases are because the flow was ignited at about 36 ms and it takes time before the entire flow field is burning. In the following discussion, we focus on one cycle of the oscillation, the cycle between 41 and 44.5 ms, during which

the entire flow field is composed of burning vortices. During this cycle, the peak in the energy release occurs at about 43.5 ms. Most of the energy is released between 42.7 and 44.1 ms which corresponds to timesteps 205000 and 215000 in Fig. 10. This correlation between the structure of the flow field and the energy release helps to identify the relation between the two. A quantative relation is discussed later.

Figure 13 shows the energy released as a function of time and space. The energy released is always minimal near the entrance to the combustor. Also, initially there is no energy release in portions of the combustor because the ignited vortex has not yet reached these locations. Locations of strong energy release move in space because the energy release is taking place in burning vortices which are being convected. Note that the temporal nonuniformity in energy release is different at different locations. One approach to summarizing the information in this figure and determining the spatial distribution of energy release is to consider the time-averaged energy release at various locations in the combustor. Figure 14 shows the time-average energy release taken over one cycle of the oscillation (determined from the flow visualisation in Figs. 9 and 10) as a function of axial location. This figure shows that most of the energy is released in the second half of the combustor, that is, the half closest to the exit nozzle. Figures 12, 13 and 14 give a picture of the temporal and spatial distribution of energy release and suggest that events occuring in the second half of this combustor between 42.7 and 44.1 ms (during one cycle) are important in assessing the global effects of energy release on the flow field.

Unsteady Pressure Fluctuations

One of the important reasons for simulating the flow fields in ramjets is to evaluate the coupling between the energy released and the pressure oscillations. Figure 15 shows the pressure fluctuations at a particular location (3.04 D from the inlet-combustor junction). There are approximately three cycles of large pressure oscillations. During the cycle of interest to us, the pressure is rising at 42 ms, attains a maximum between 42.7 and 43.5 ms, and then decreases to a minimum at about 45 ms. The fourier analysis of this data and similar data at six different locations in the combustor show that tha large-amplitude

oscillations are at about 280 Hz. The cause of these large pressure oscillations is the strong coupling between the pressure and the unsteady energy release.

Rayleigh's Criterion

A criterion first proposed by Lord Rayleigh [30] is a convenient method for evaluating the interaction between the energy released and the pressure waves in the system. Rayleigh's criterion states that presssure oscillations will be amplified if the energy release is in phase with the pressure and will be diminished if they are out of phase. The frequency will be affected if the energy release occurs at a quarter period before or after the maximum pressure. In a complex flow field such as that in the combustor discussed here, the unsteady energy release and the pressure fluctuations do not have simple waveforms and hence the phase relation between the two can vary from one location to another. In this context, Rayleigh's criterion implies that the instability is *locally amplified* if the unsteady energy release $e'_r(x,t)$ and pressure fluctuation $p'(x,t)$ are in phase. More generally, if we define

$$D(x) = \frac{1}{T} \int_T e'_r(x,t) p'(x,t) dt \tag{7}$$

where T refers to the period under consideration. Local amplification (or driving) occurs if $D(x)$ is positive and local attenuation (or damping) occurs if $D(x)$ is negative.

In principle, we can evaluate $D(x)$ at all locations in the combustor if we know e'_r and p' at all locations through out the cycle. Because of the large amount of data required, it is impractical to evaluate this criterion at all locations (or volume elements) in the combustor. Therefore, we discretized the combustor into a series of axial stations and evaluated the criterion at these stations. A station is defined as a slice through the combustor and has the thickness of an axial computational cell. The drawback with this approach is that all radial variations in the energy released are averaged out. The pressure fluctuations used are those calculated at half the radius of the combustor because the radial variations in the pressure are not significant in this problem which is dominated by longitudinal

oscillations. The integrand in the above equation evaluated at a particular station 3.04 D is shown as a function of time in Fig. 16. Most of the time, there is only slight driving (positive values) or damping (negative values) but there is strong driving between 43.1 and 43.4 ms. The net value (given by the area under the curve) is positive, indicating that the pressure oscillations are driven at this station. The experiments of Hegde et. al.[31] have shown that it is important to consider the coupling over the entire combustor because the oscillations may be damped at certain locations while being amplified at other locations. The total effect over the whole combustor can be determined by evaluating the criterion at various axial stations in the combustor and integrating it over the whole combustor. Figure 17 indicates that there is damping at axial locations up to about 2.3 D over the cycle considered. Locations between 3 and 4.5 D are strongly driving the oscillations. Similar results have been obtained over other cycles of oscillations indicating that the ramjet is operating in an unstable mode for the conditions considered in this simulation.

Effects of Pre-Energy Release Reactions

As discussed in the numerical model section, the chemistry has been modelled using a two-step phenomenological model. The first step models the induction or pre-energy release reactions. This step is necessary to account for the finite time, called the induction time, that is required for a heated mixture to begin releasing its chemical energy. Induction times are a function of the local temperature, pressure and stoichiometry of the mixture. The induction times data used in these simulations are a function of the local temperature and pressure but depend only on the initial stoichiometry of the mixture. In some situations, convective mixing can change the local stoichiometry (by for example, an influx of radicals) before the elapse of the induction period. Therefore, it is important to assess the sensitivity of the results presented above to variations in the induction time due to compositional changes.

Starting from the same cold-flow simulations at step 160000, we have performed a new reactive flow simulation in which all of the local induction times were reduced by a factor of ten. The rate of energy release and the amount of energy released were not changed. The

19

time evolution of temperature is shown at a subsequent sequence of times in Fig. 18 and the vortical flowfield in Fig. 19. We note that the flow field is still composed of a few large scale structures. Some of the more convoluted temperature contours observed in Figs. 9a and 10 a for the previous case have become less convoluted because of the earlier elapse of induction time in this case. Comparing the solutions at corresponding times in the two cases shows that although the temperature contours are less curved in this case than in the previous one, the flow field is still dominated by a large-scale vortex. A noticeable difference from the previous case is that most of the energy is released in the middle two-thirds of the combustor. However, as shown in Fig. 20, the pressure fluctuations at a particular location in the combustor are not very different in the two cases. Performing a detailed analysis of the coupling between energy release and pressure fluctuations as before shows that the combustor is still operating in an unstable mode. The results of this analysis are shown in Fig. 21. The fact that the overall results did not change significantly even though the actual shape of the high-temperature front is changed, suggests that the fine-details of the mixing process is not important for the problem discussed here. From this test, we also conclude that the pre-energy release chemistry described by the induction time does not play a dominant role in combustion instabilities in the system investigated in this paper.

4. SUMMARY AND CONCLUSIONS

In this paper, we first presented numerical simulations of vortex-shedding and merging in an axisymmetric combustor for a nonreactive flow and then presented simulations in which there was energy release from chemical reactions. The nonreactive flow calculations show complex interactions among the natural instability frequency of the shear layer at the inlet-combustor junction and the acoustics of the inlet and the combustor. For the particular reactive flow case studied, energy release alters the flow field substantially and amplifies the low-frequency oscillation observed in the nonreactive flow.

In the nonreactive flow simulations, vortex-shedding occurs at the natural instability frequency of the initially laminar shear layer. This is consistent with the observation made earlier that if the natural instability frequency is much higher than the first longitudinal mode frequency, then vortex shedding takes place at the shear-layer instability frequency [11].

Two successively generated vortices merge within one diameter of the inlet-combustor junction. This frequency is nearly one-half of the vortex-shedding frequency. A complex pattern of vortex-mergings occur in the second half of the combustor. Vortex mergings occur at both the first longitudinal mode frequency of the combustor as well as at a lower frequency. This lower frequency is probably a beat frequency between the quarter-wave mode frequency in the inlet and the first longitudinal mode frequency of the combustor. Vortex mergings are also occasionally observed at frequencies higher than the first longitudinal mode frequency.

The entire flow is quasi-periodic at the quarter-wave mode frequency of the inlet. This, coupled with observations from previous simulations [8,10,12], suggests that the overall periodicity of the flow field in an axisymmetric combustor is that of the lowest dominant frequency of the system. In this particular simulation, the flow is quasi-periodic instead of periodic because of a mismatch between the various competing frequencies. In a previous simulation [12], for which there were only two dominant frequencies in the system and one was an integral multiple of the other, the flow showed very little variation from

cycle to cycle.

The simulations with chemical reactions show that energy release alters the flow field in the combustor substantially. In the first cycle after ignition, fluid expansion due to energy release quickly destroys the pattern of vortex mergings observed in the cold flow and a new pattern emerges that is dominated by a large vortex. In subsequent cycles, most of the energy release occurs after vortex mergings have produced this large vortex. Energy release in this large vortex is in phase with the pressure oscillation over a substantial region of the combustor between the axial stations 2.5 to about 5 D. This results in the observed amplification of the low-frequency oscillations and leads to combustion instability.

In the second case with energy release, we studied the effects of changing one of the chemistry parameters. The induction time which models the pre-energy release chemistry was reduced by a factor of ten. This resulted in some changes in the details of the flow field but did not alter the level of pressure fluctuations substantially. This study indicates that pre-energy release chemistry does not play a dominant role in combustion instabilities in the combustion system studied here. It also highlights the dominant role played by the energy release chemistry and the need to model it adequately.

Both of the reactive flow simulations show that there are regions in the combustor where the oscillations are damped. This suggests that combustion instability may be controllable by dynamically controlling the phase relation between the unsteady energy release and the pressure fluctuations and hence increasing the size of the regions where the oscillations are damped. Several approaches to controlling the combustion instability as well as additional parametric studies of the effects of chemistry are currently being persued.

5.ACKNOWLEDGEMENTS

6. REFERENCES

1. Kailasanath, K., Gardner, J.H., Boris, J.P. and Oran, E.S., "Numerical Simulations of the Flowfield in a Central-Dump Ramjet Combustor—I. Tests of the Model and Effects of Forcing," NRL Memorandum Report 5832, Naval Research Laboratory, Washington, D.C., 1986.

2. Kailasanath, K., Gardner, J.H., Boris, J.P. and Oran, E.S., "Numerical Simulations of the Flowfield in Central-Dump Ramjet Combustors—II. Effects of Inlet and Combustor Acoustics," NRL Memorandum Report 6213, Naval Research Laboratory, Washington, D.C., 1988.

3. Ashurst, W.T., "Vortex Simulation of a Model Turbulent Combustor," *Prog. Astro. Aero.*, Vol. 76, 1981, pp. 259-273.

4. Ghoniem, A.F., Chorin, A.J. and Oppenheim, A.K., "Numerical Modeling of Turbulent Combustion in Premixed Gases," *Eighteenth Symposium (International) on Combustion*, The Combustion Institute, Pittsburgh, 1981, pp. 1375-1383.

5. Ghoniem, A.F., "Effect of Large Scale Structures on Turbulent Flame Propagation," *Combust. Flame*, Vol. 64, 1986, pp. 321-336.

6. Scott, J.N., and Hankey, W.L., "Numerical Simulation of Cold Flow in an Axisymmetric Centerbody Combustor," *AIAA Journal*, Vol. 23, May 1985, pp. 641-649.

7. Drummond, J.P., "Numerical Study of a Ramjet Dump Combustor Flowfield," *AIAA Journal*, Vol. 23, Apr. 1985, pp. 604-611.

8. Kailasanath, K., Gardner, J.H., Boris, J.P. and Oran, E.S., "Acoustic-Vortex Interactions in an Idealized Ramjet Combustor," *Proceedings of the 22nd JANNAF Combustion Meeting, Pasadena, CA*, CPIA publication 432, Vol. 1, Oct. 1985, pp. 341-350.

9. Jou, W.H. and Menon, S., "Large Eddy Simulations of Flow in a Ramjet Combustor," *Proceedings of the 22nd JANNAF Combustion Meeting, Pasadena, CA*, CPIA publication 432, Vol. 1, Oct. 1985, pp. 331-339.

10. Kailasanath, K., Gardner, J., Boris, J. and Oran, E., "Interactions Between Acoustics and Vortex Structures in a Central Dump Combustor," AIAA paper 86-1609, also see *J. Prop. Power*, Vol. 3, Nov-Dec. 1987, pp. 525-533.

11. Kailasanath, K., Gardner, J.H., Oran, E.S., and Boris, J.P. "Numerical Simulations of High-Speed Flows in an Axisymmetric Ramjet," AIAA paper 88-0339, AIAA 26th Aerospace Sciences Meeting, Reno, Jan. 1988, AIAA, Washington, D.C.

12. Kailasanath, K., Gardner, J.H., Boris, J.P., and Oran, E.S., "Acoustic-Vortex Interactions and Low Frequency Oscillations in Axisymmetric Combustors," AIAA paper 87-0165, AIAA 25th Aerospace Sciences Meeting, Reno, Jan. 1987 (also to appear in *J. Prop.Power.*, 1989).

13. Kailasanath, K., Gardner, J.H., Oran, E.S. and Boris, J.P., "Numerical Simulations of the Reactive Flow Field in an Axisymmetric Combustor," AIAA paper 87-1423, AIAA 19th Fluid Dynamics, Plasma Dynamics and Lasers Conference, Honolulu, HA, June 1987, AIAA, Washington, D.C.

14. Sivasegaram, S. and Whitelaw, J.H.,"Oscillations in Axisymmetric Dump Combustors," *Combust. Sci. and Tech.* 52, pp. 413-426.

15. Oran, E.S. and Boris, J.P.,"Detailed Modelling of Combustion Systems," *Prog. Energy Combustion Sci.* 7, 1.

16. Boris, J.P. and Book, D.L., "Solution of Continuity Equations by the Method of Flux-Corrected Transport," *Methods of Computational Physics*, Academic Press, New York, 1976, Vol. 16, Chap. 11, pp. 85-129.

17. Oran, E.S., Young, T.R. and Boris, J.P., "Application of Time- Dependent Numerical Methods to the Description of Reactive Shocks," *Seventeenth Symposium (International) on Combustion*, The Combustion Institute, Pittsburgh, 1979, pp. 43-54.

18. Kailasanath, K., Oran, E.S., Boris, J.P. and Young, T.R., "A Computational Method for Determining Detonation Cell Size," AIAA paper No. 85-0236, AIAA 23rd Aerospace Sciences Meeting, Reno, NV, Jan. 1985, AIAA, Washington, D.C.

19. Guirguis, R.H., Grinstein, F.F., Young, T.R., Oran, E.S., Kailasanath, K., and Boris, J.P., "Mixing Enhancement in Supersonic Shear Layers," AIAA paper 87-0373, AIAA 25th Aerospace Sciences Meeting, Reno, NV, Jan. 1987, AIAA, Washington, D.C.

20. Boris, J.P., Oran, E.S., Gardner, J.H., Grinstein, F.F., and Oswald, C.E. "Direct Simulations of Spatially Evolving Compressible Turbulence—Techniques and Results," *Ninth International Conference on Numerical Methods in Fluid Dynamics*, pp. 98-102. Springer-Verlag, 1985.

21. Grinstein, F.F., Oran, E.S. and Boris, J.P., "Direct Simulation of Asymmetric Mixing in Planar Shear Flows," *J. Fluid Mech.*, Vol. 165, 1986, pp. 201-220.

22. Burks, T.L., and Oran, E.S., "A Computational Study of the Chemical Kinetics of Hydrogen Combustion," NRL Memorandum Report 4446, Naval Research Laboratory, Washington, D.C., 1981.

23. Oran, E.S., Boris, J.P., Young, T., Flanigan, M., Burks, T., and Picone, M., "Numerical Simulations of Detonations in Hydrogen-air and Methane-air Mixtures," *Eighteenth Symposium (International) on Combustion*, The Combustion Institute, Pittsburgh, 1981, pp. 1641-1649.

24. Paczko, G., Lefdal, P.M., and Peters, N., "Reduced Reaction Schemes for Methane, Methanol and Propane Flames," *Twentyfirst Symposium (International) on Combustion*, The Combustion Institute, Pittsburgh, 1988, pp. 739-748.

25. Frenklach, M., (Penn. State University), Private Communication, 1988.

26. Kailasanath, K., Oran, E.S., Boris, J.P., and Young, T., "Determination of Detonation Cell Size and the Role of Transverse Waves in Two-Dimensional Detonations," *Combust. Flame* 61:199-209 (1985).

27. Shapiro, A.H., *The Dynamics and Thermodynamics of Compressible Fluid Flow*, The Ronald Press Company, New York, 1953, Vol. I, pp. 83-84.

28. Zaman, K.B.M.Q., and Hussain, A.K.M.F., "Vortex Pairing in a Circular Jet Under Controlled Excitation. Part 1. General Jet Response," *J. Fluid Mech.*, Vol. 101, 1980,

pp. 441-449.

29. Michalke, A., "On Spatially Growing Disturbances in an Inviscid Shear Layer," *J. Fluid Mech.*, Vol. 23, 1965, pp. 521-544.

30. Rayleigh, J.W.S., "The Explanation of Certain Acoustical Phenomena," *Nature* , Vol. 18, 1878, p. 319; also see *Theory of Sound*, Vol. II, pp. 224-235, Dover, New York, 1945.

31. Hegde, U.G., Reuter, D., Daniel, B.R. and Zinn, B.T., "Flame Driving of Longitudinal Instabilities in Dump Type Ramjet Combustors," *Combust. Sci. and Tech.*, Vol. 55, 1987, pp. 125-138.
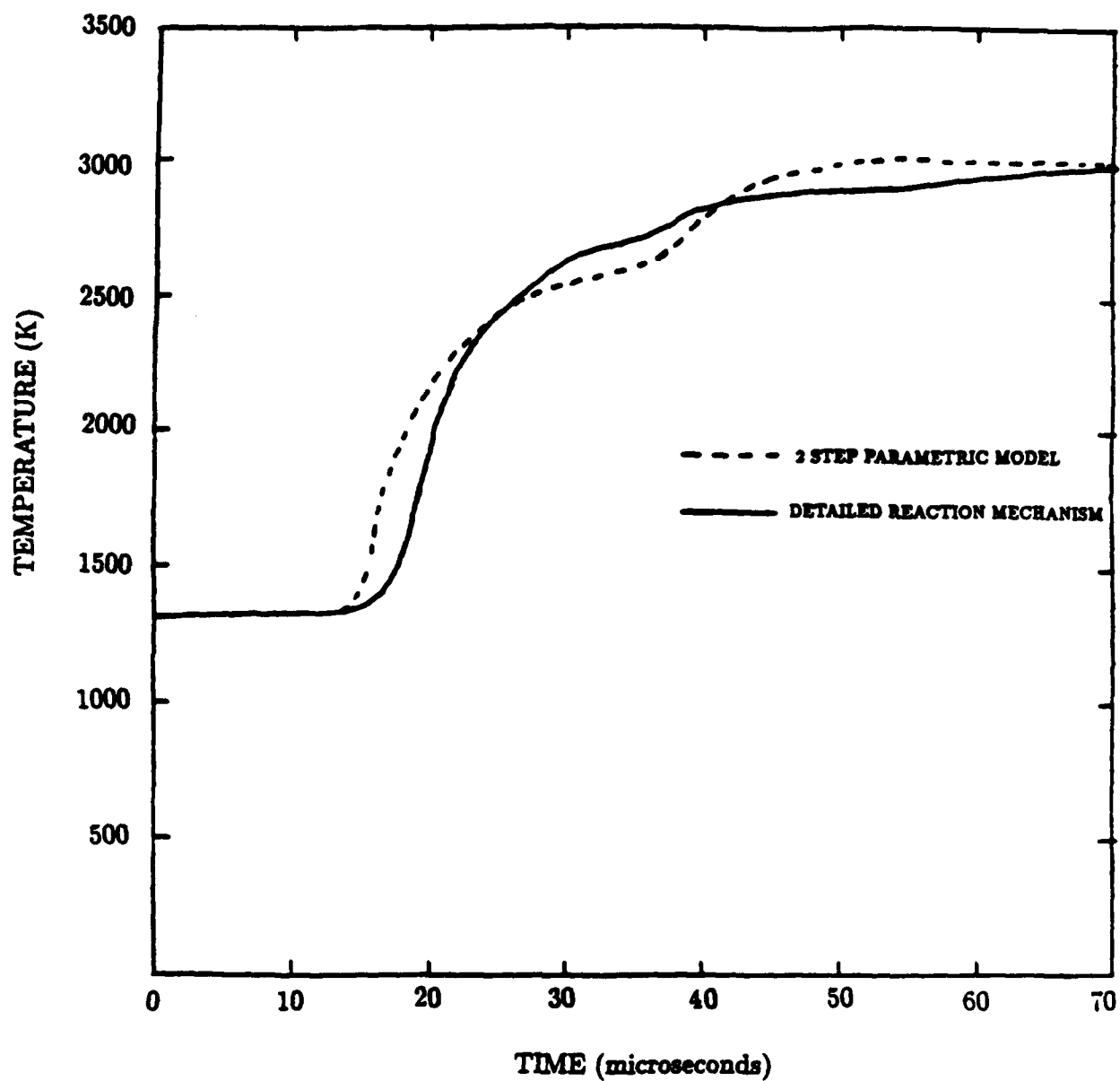
Fig. 1a — Comparison of the time-history of temperature behind a shock calculated using two different chemistry models
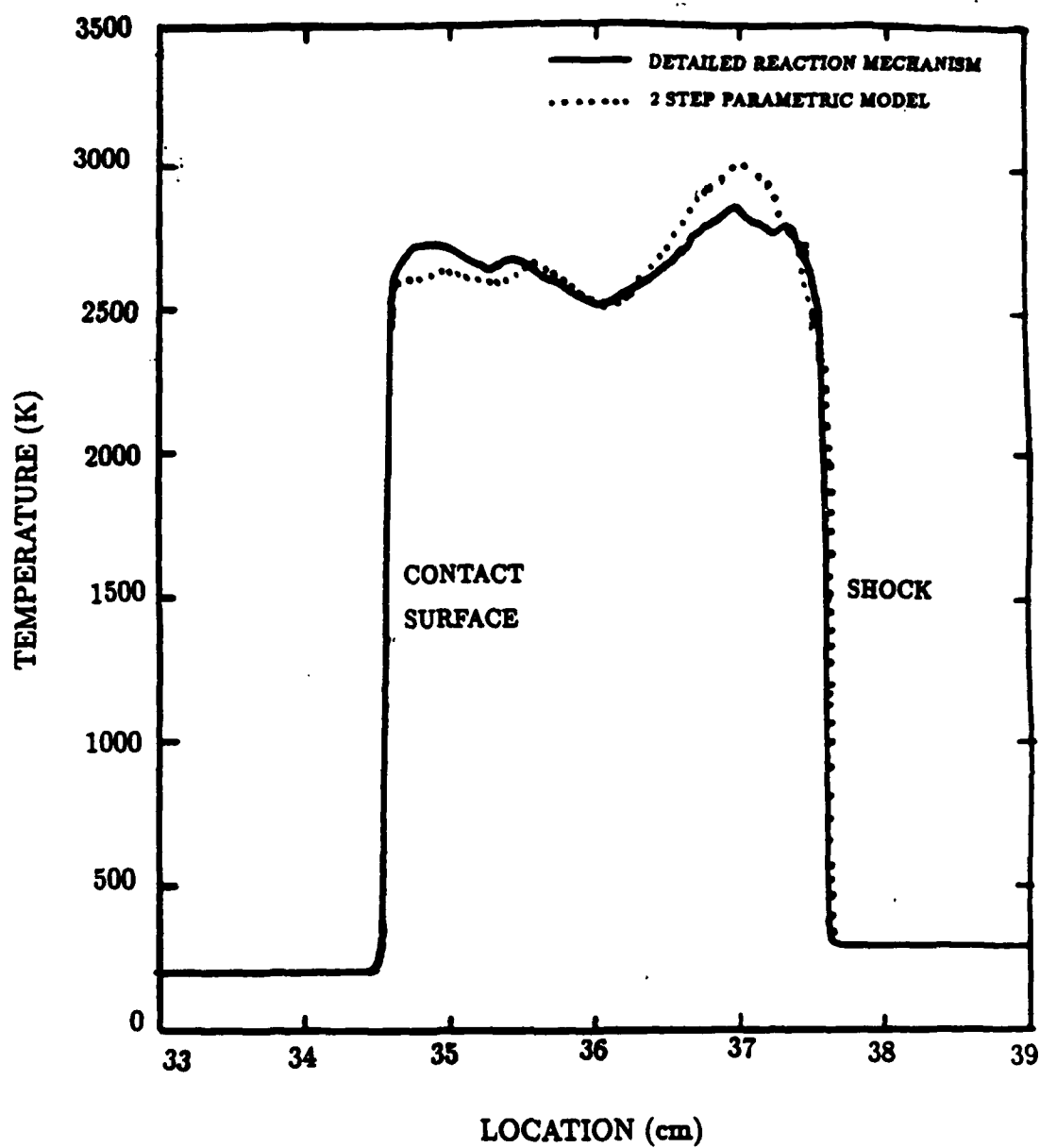
Fig. 1b — Comparison of the spatial distribution of temperature in a shock-tube at a particular time calculated using the two different chemistry models
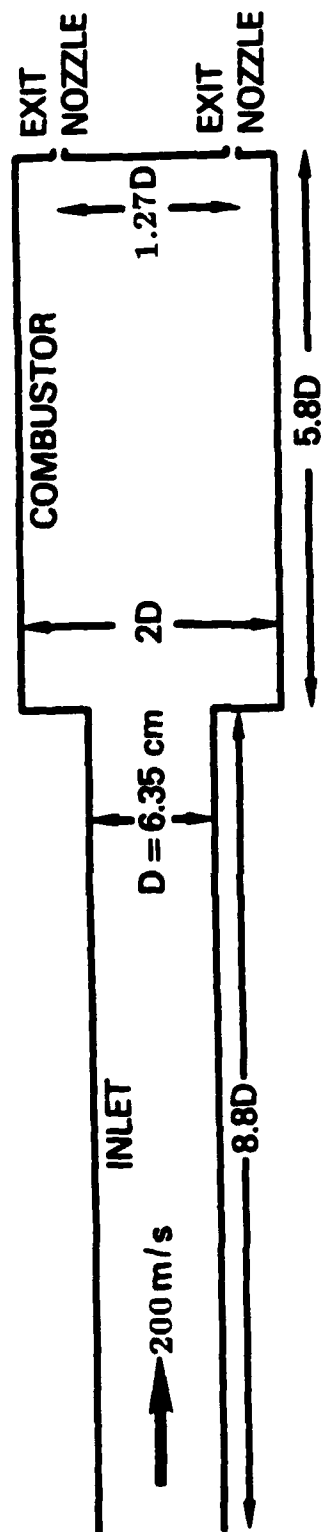
Fig. 2 — Basic configuration of the idealized axisymmmetric ramjet combustor
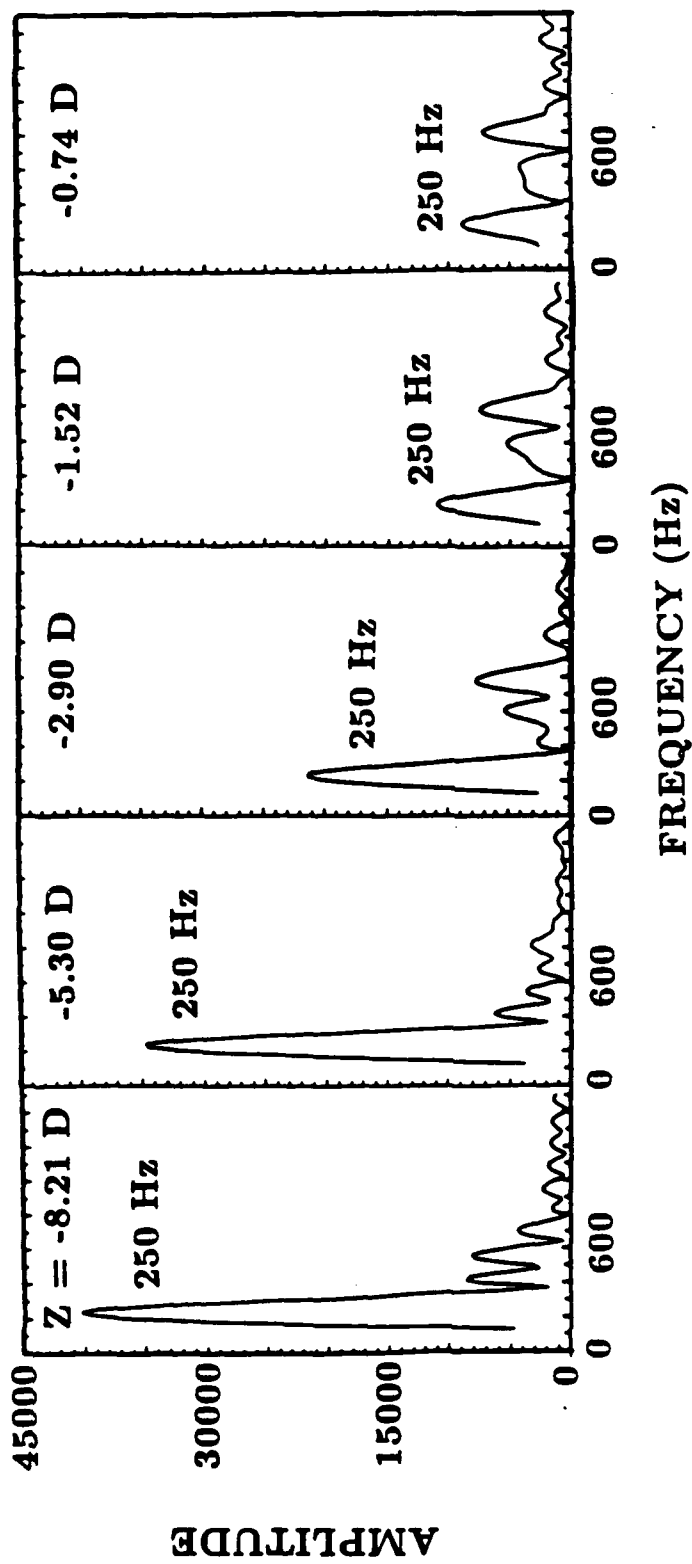
Fig. 3 — Frequency spectra of pressure fluctuations at five axial locations in the inlet

31

TIME (ms)
STEP

1   22.83
     100500

2   26.85
     118500

3   30.74
     136000

4   34.30
     152000
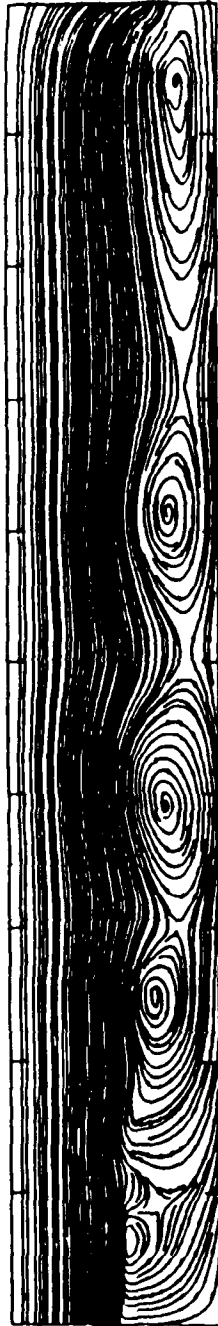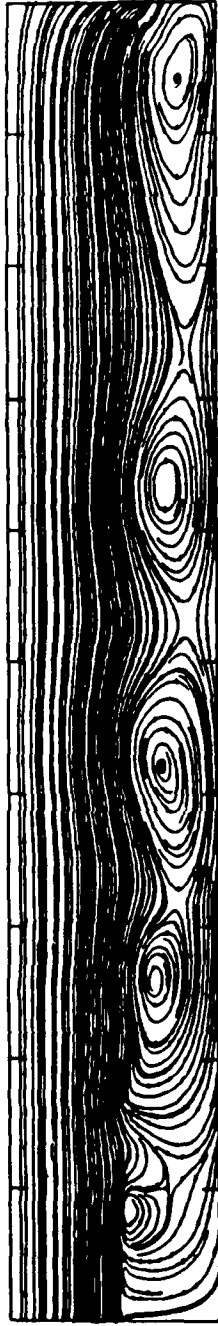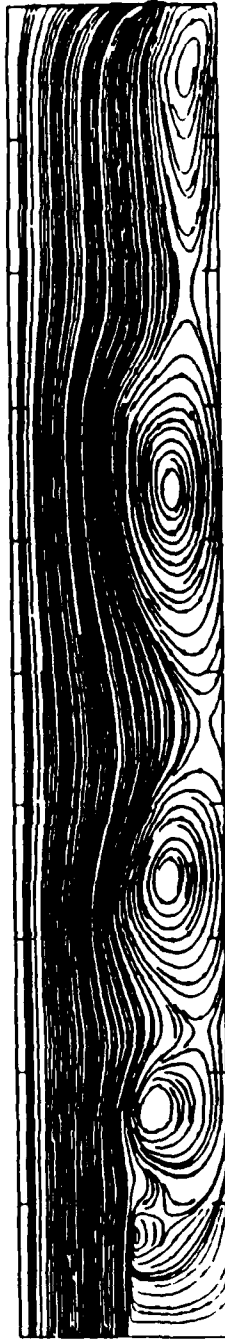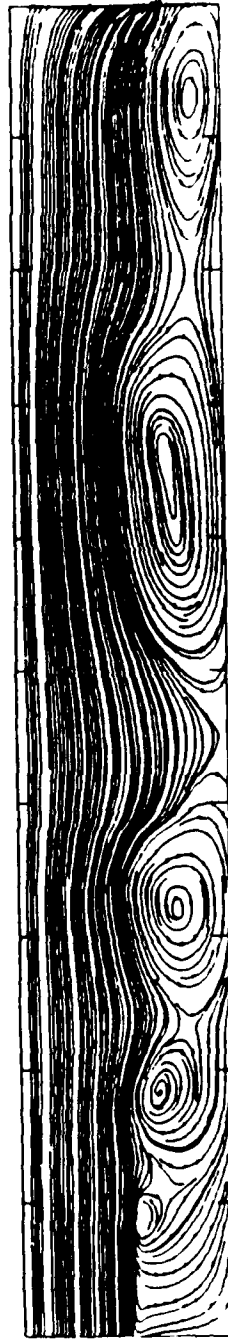
Fig. 4 — Streamlines showing the instantaneous flow field at a sequence of timesteps when the overall flow pattern is similar

32
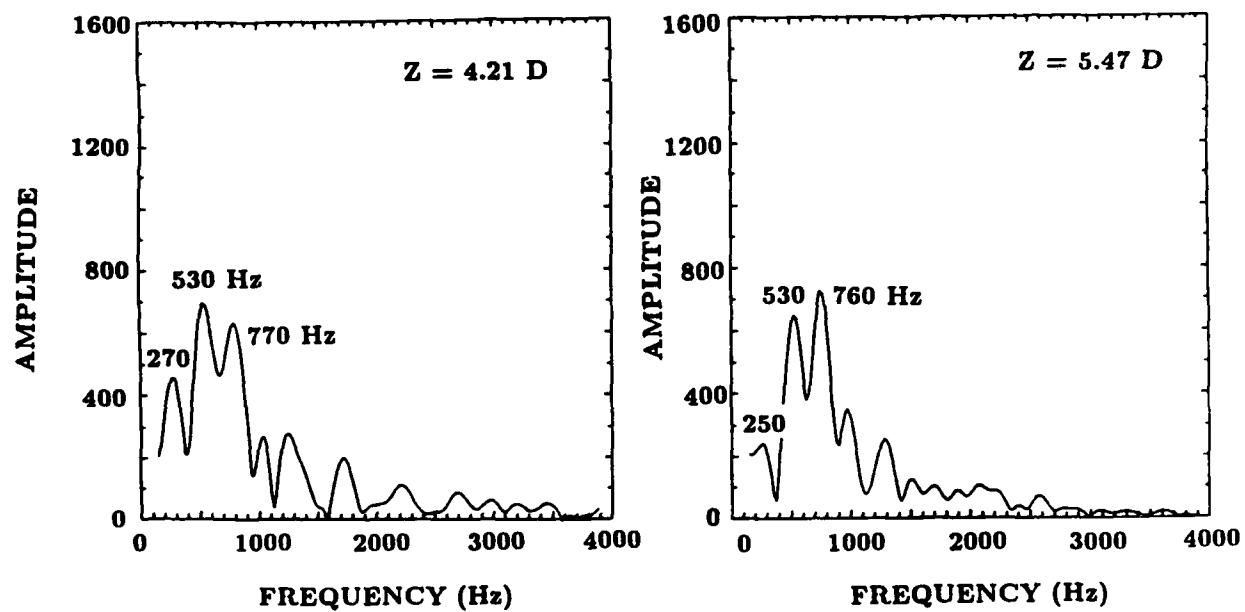
Fig. 5 — Frequency spectra of velocity fluctuation in the shear layer at two locations between which vortex mergings are observed

TIME (ms)
STEP

20.48
90000   1

21.82
96000   2

23.16
102000   3

24.05
106000   4

25.39
112000   5

27.29
120500   6

28.07
124000   7

29.41
130000   8
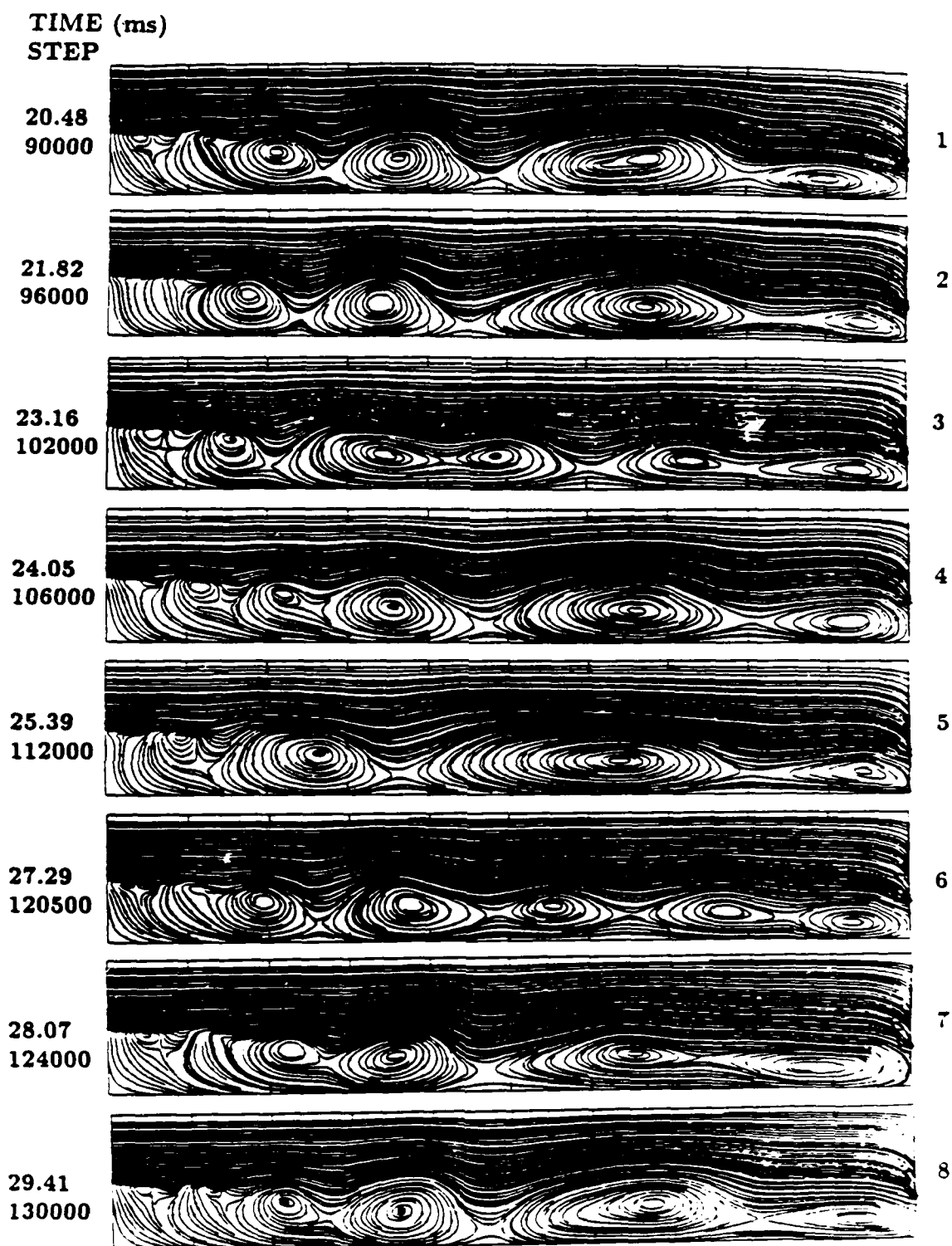
Fig. 6 — Streamlines showing the instantaneous flow field at a sequence of times when vortex mergings are observed in the
second half of the combustor
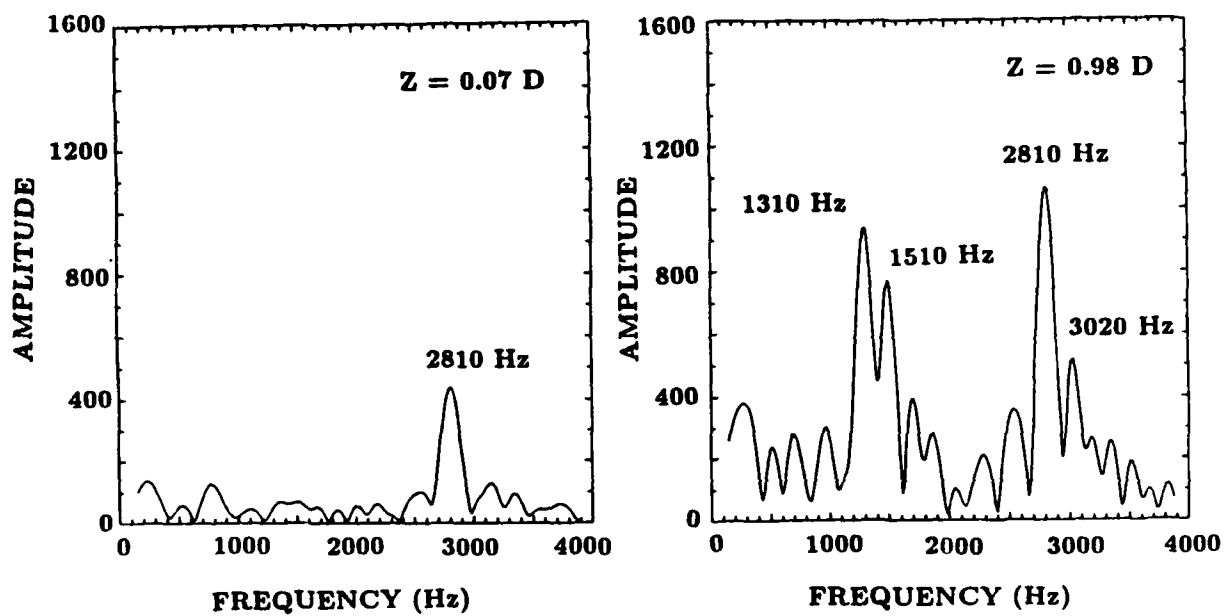
Fig. 7 — Frequency spectra of velocity fluctuations in the shear layer at two locations near the combustor-step
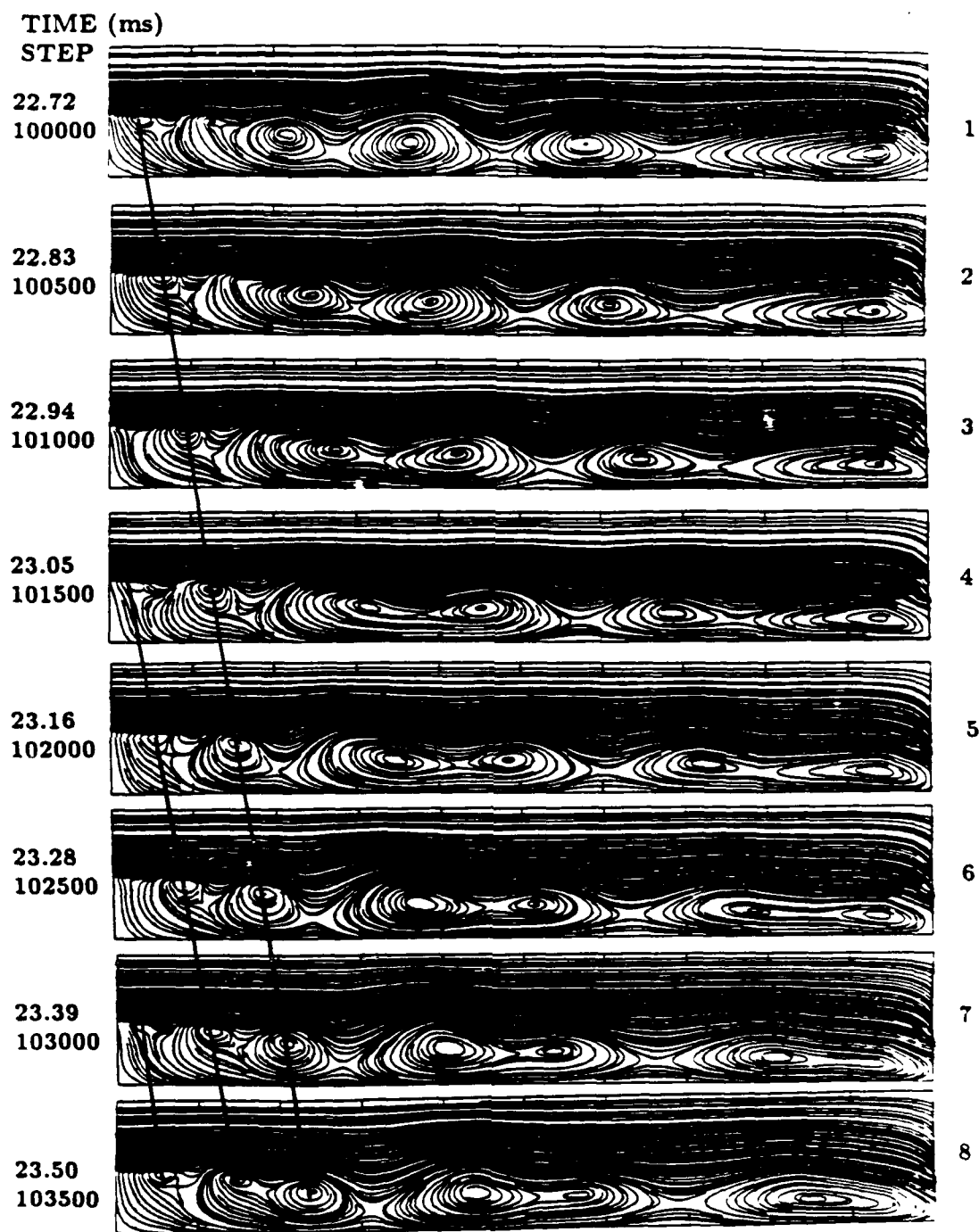
Fig. 8 — Streamlines showing vortex shedding and merging near the combustor-step
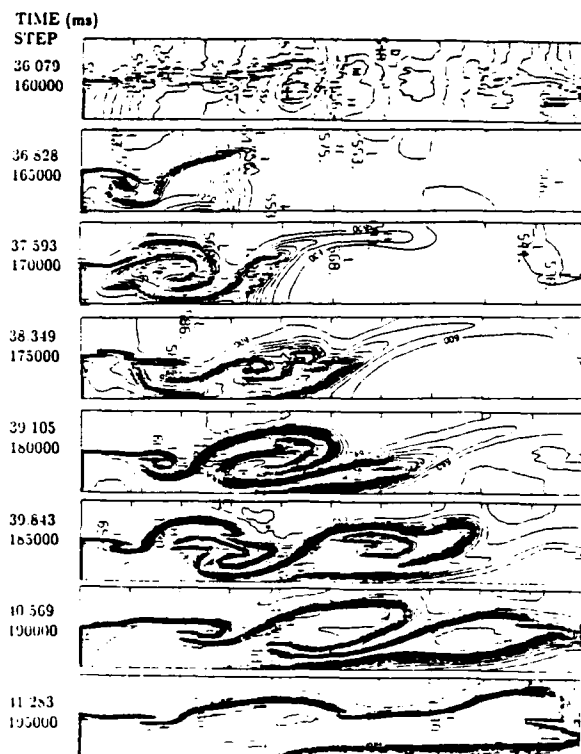
Fig. 9a — Temperature contours showing the instantaneous flow field at a sequence of timesteps in the early stages of the reactive flow case. The mixture is ignited at the end of timestep 160000.
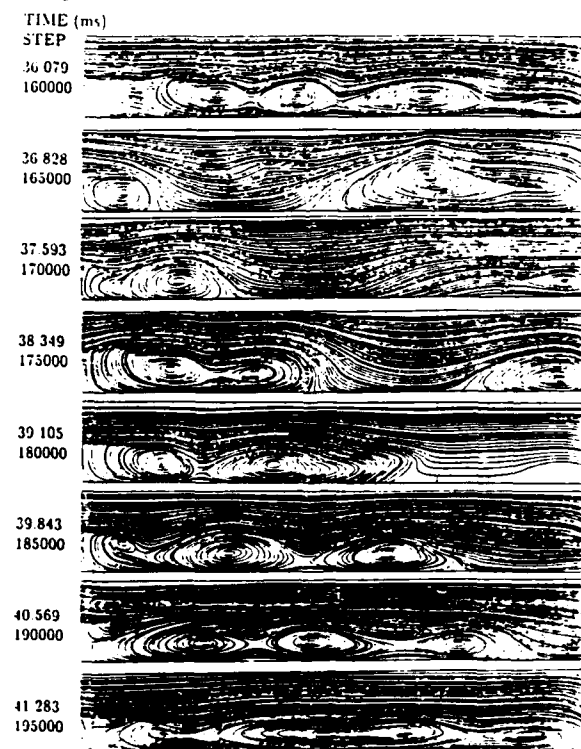
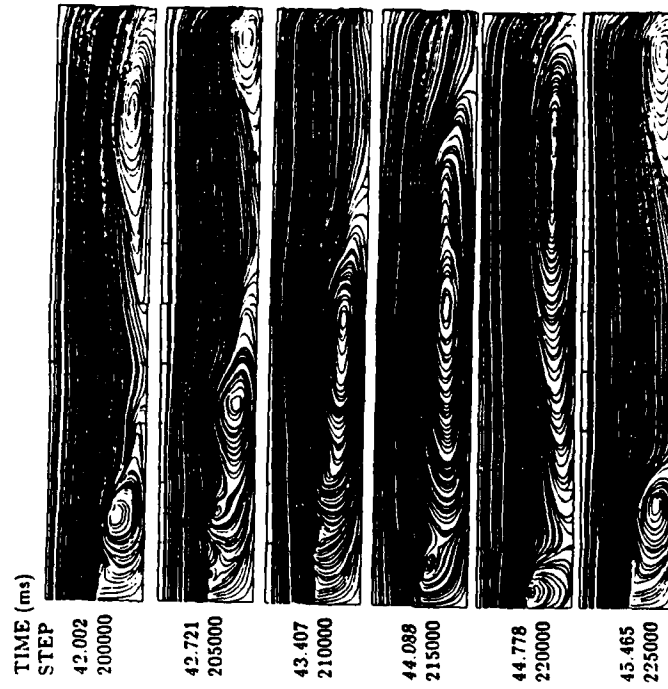Fig. 9b — Streamlines corresponding to the temperature contours in Fig. 9a

37

Fig. 10a — Temperature contours showing the instantaneous flow field at a sequence of timesteps in the later stages of the reactive flow case

Fig. 10b — Streamlines corresponding to the temperature contours in Fig. 10a

Reactive Flow

TIME (ms)
STEP

42.002
200000

42.721
205000

43.407
210000

44.088
215000

44.778
220000

45.465
225000

Cold Flow

TIME (ms)
STEP

30.744
136000

31.189
138000

31.632
140000

32.075
142000

32.520
144000

32.965
146000

33.410
148000

33.855
150000

34.301
152000

Fig. 11 — Streamlines showing a comparison of the flowfields in the cold-flow and reactive-flow cases

39
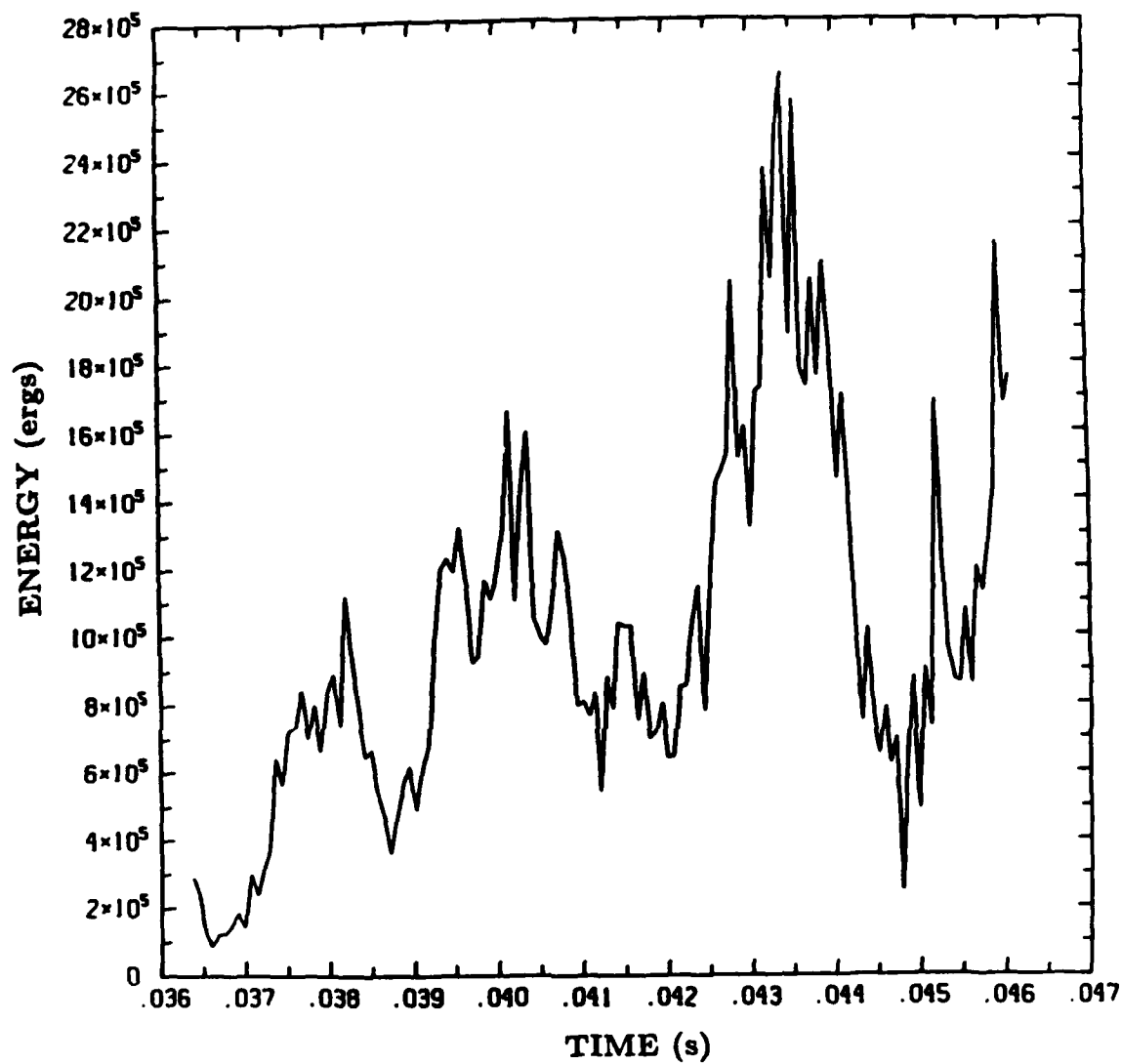
Fig. 12 — Total energy released in the combustor as a function of time
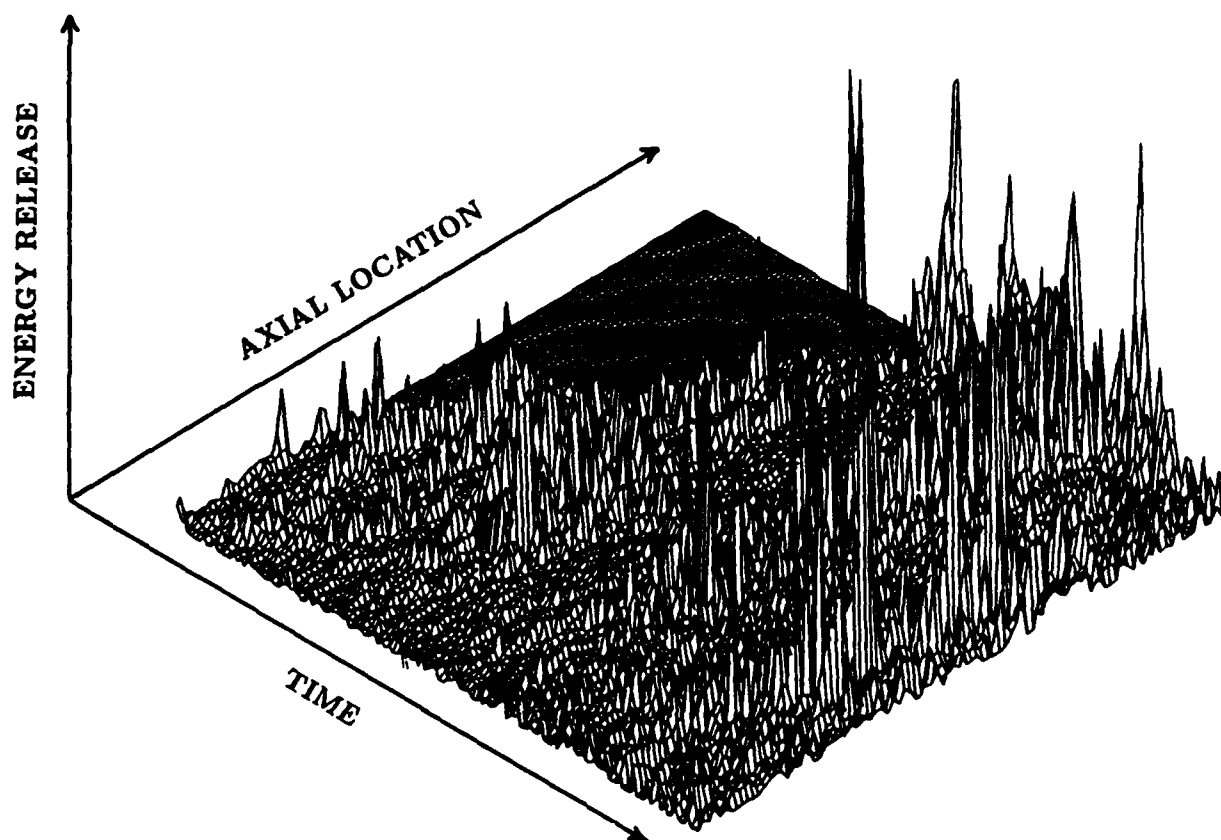
Fig. 13 — Temporal variation of instantaneous energy release at various axial stations in the combustor

41
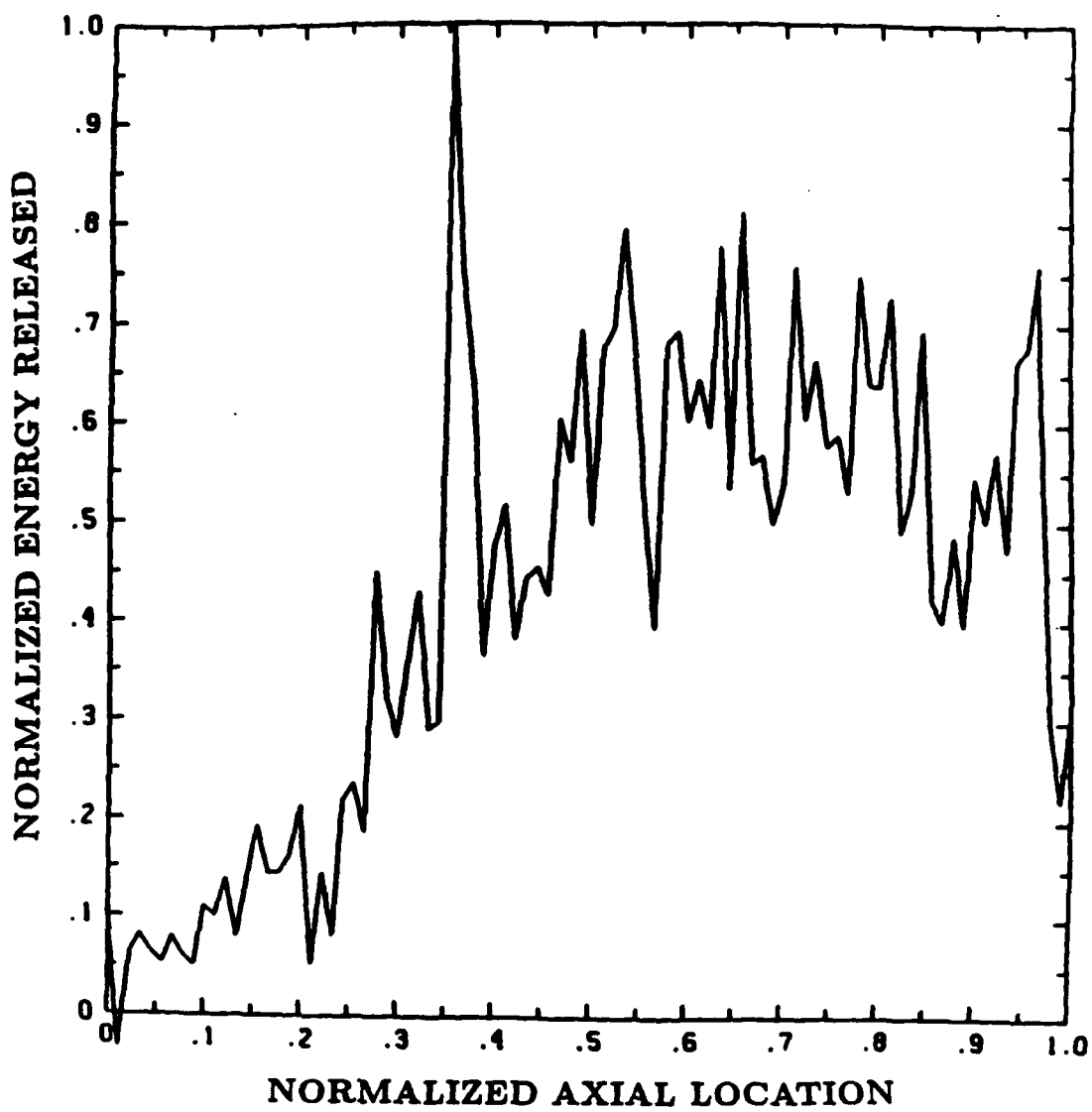
Fig. 14 — Time-averaged energy released at various axial stations in the combustor
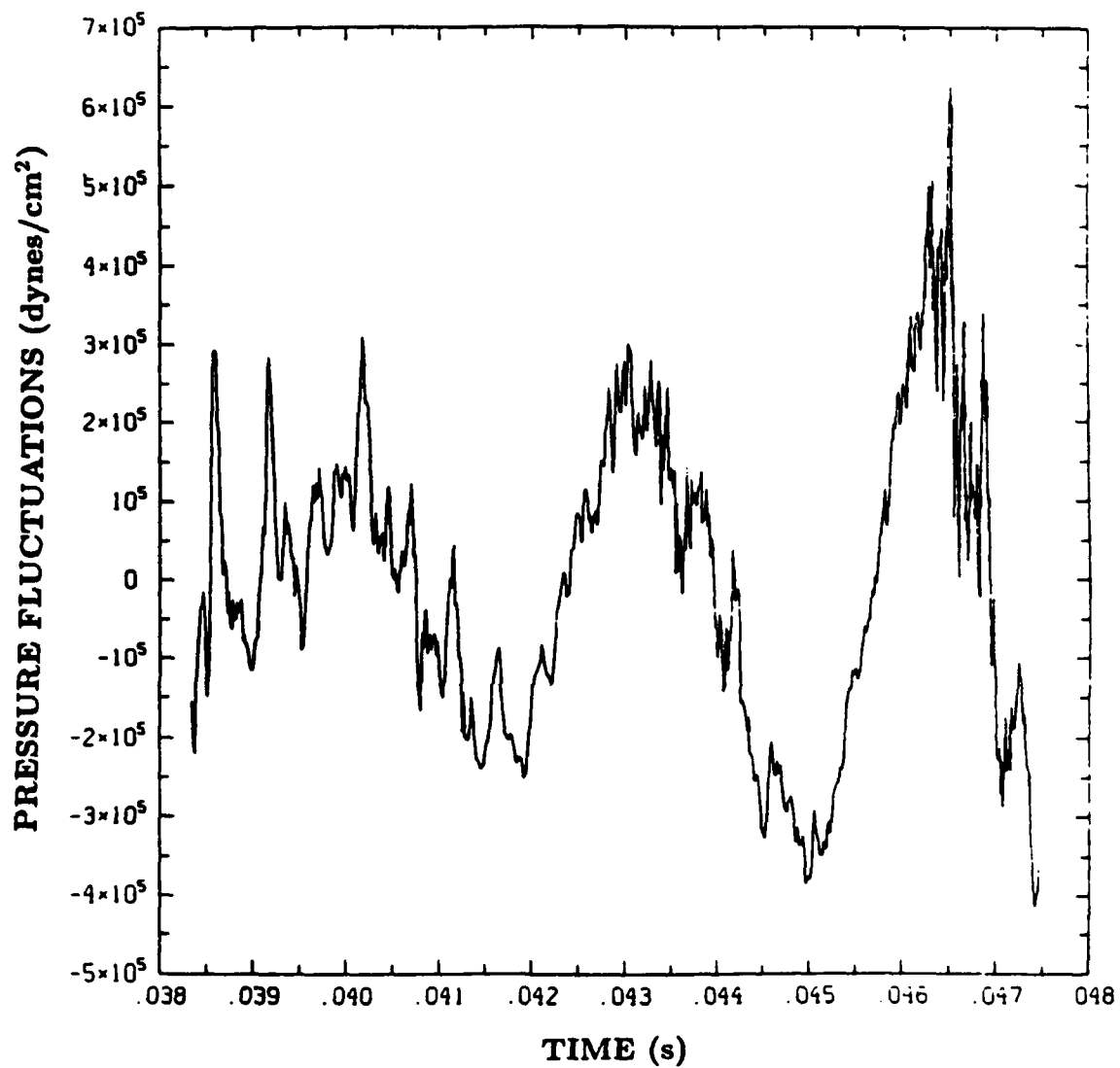
Fig. 15 — Time evolution of instantaneous pressure fluctuations at a particular location (3.04 D) in the combustor
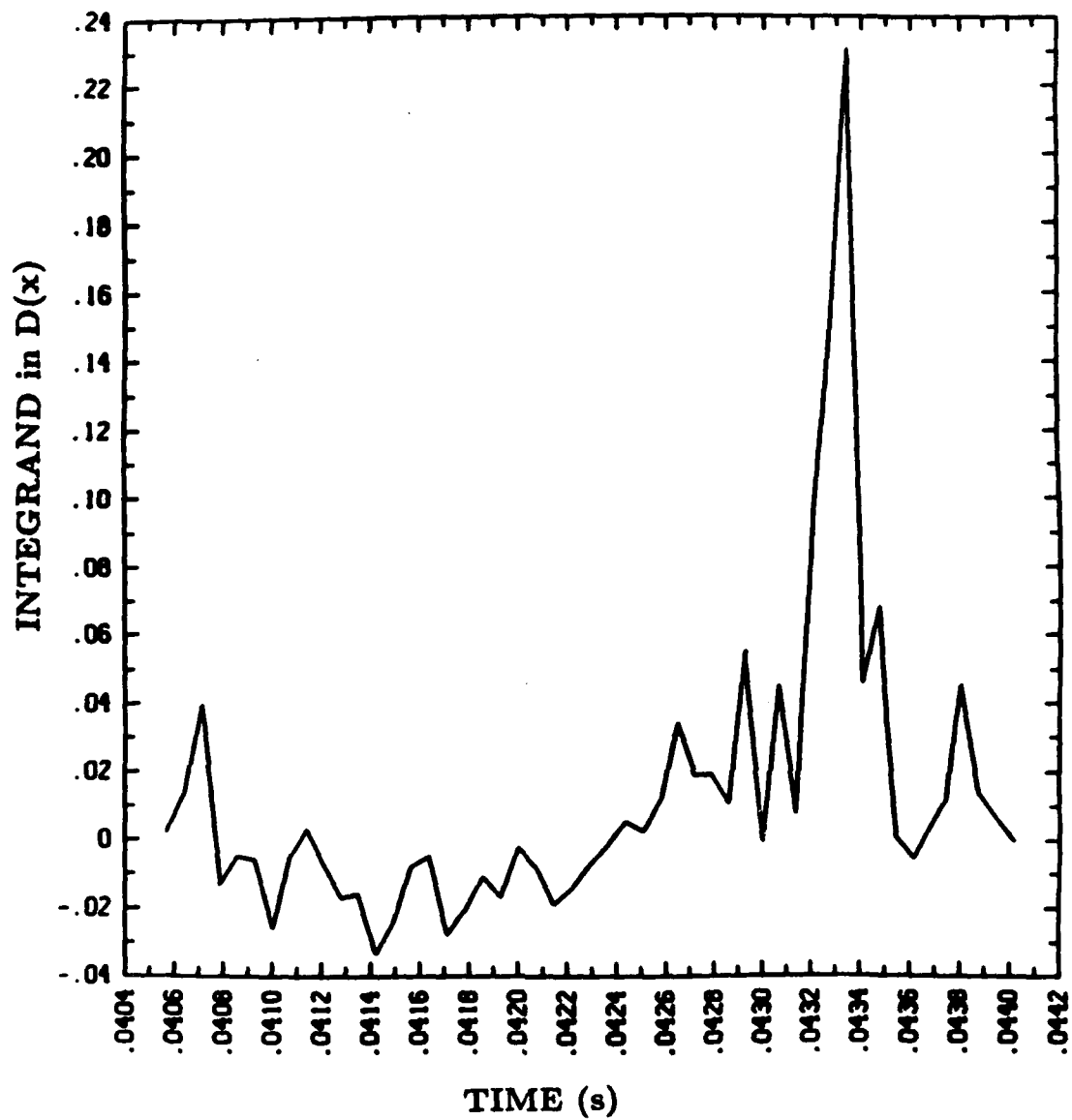
Fig. 16 — Time evolution of the integral expressing Rayleigh's criterion at a particular station (3.04 D) in the combustor
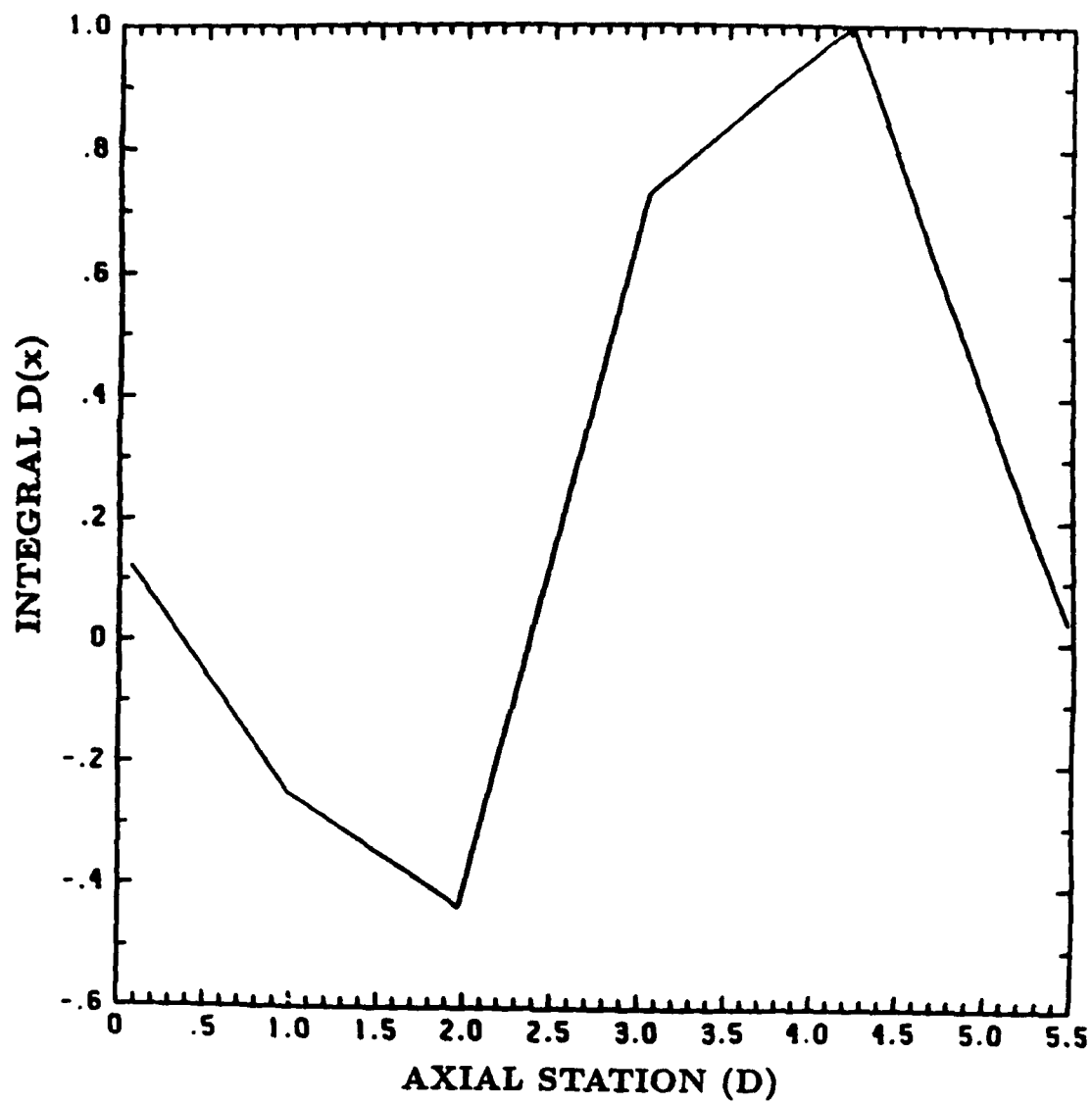
Fig. 17 — Time-averaged value of the integral expressing Rayleigh's criterion at a series of axial stations in the combustor
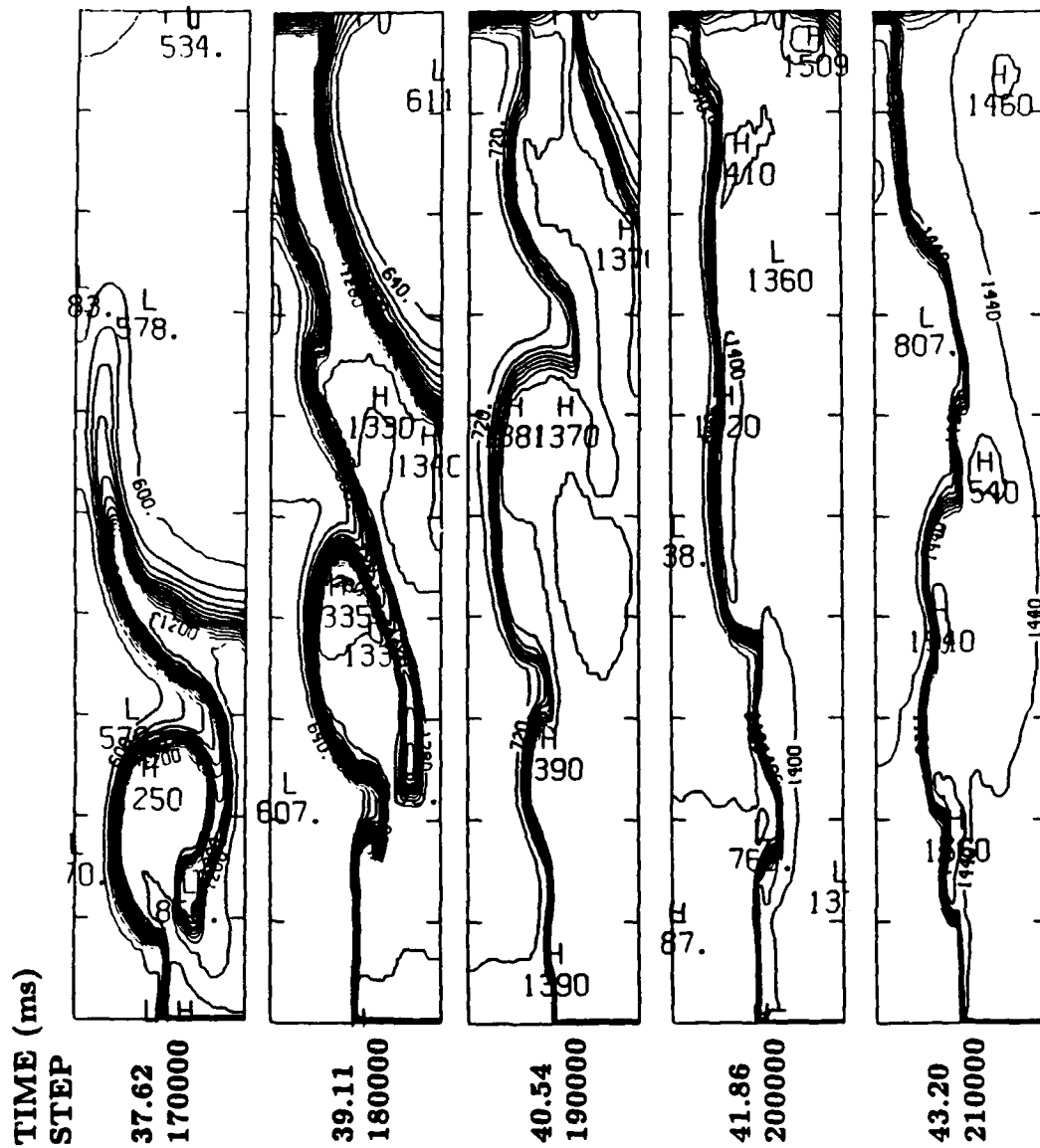
Fig. 18 — Temperature contours showing the instantaneous flow field at a sequence of times in the reactive flow case in which the induction time is reduced by a factor of ten
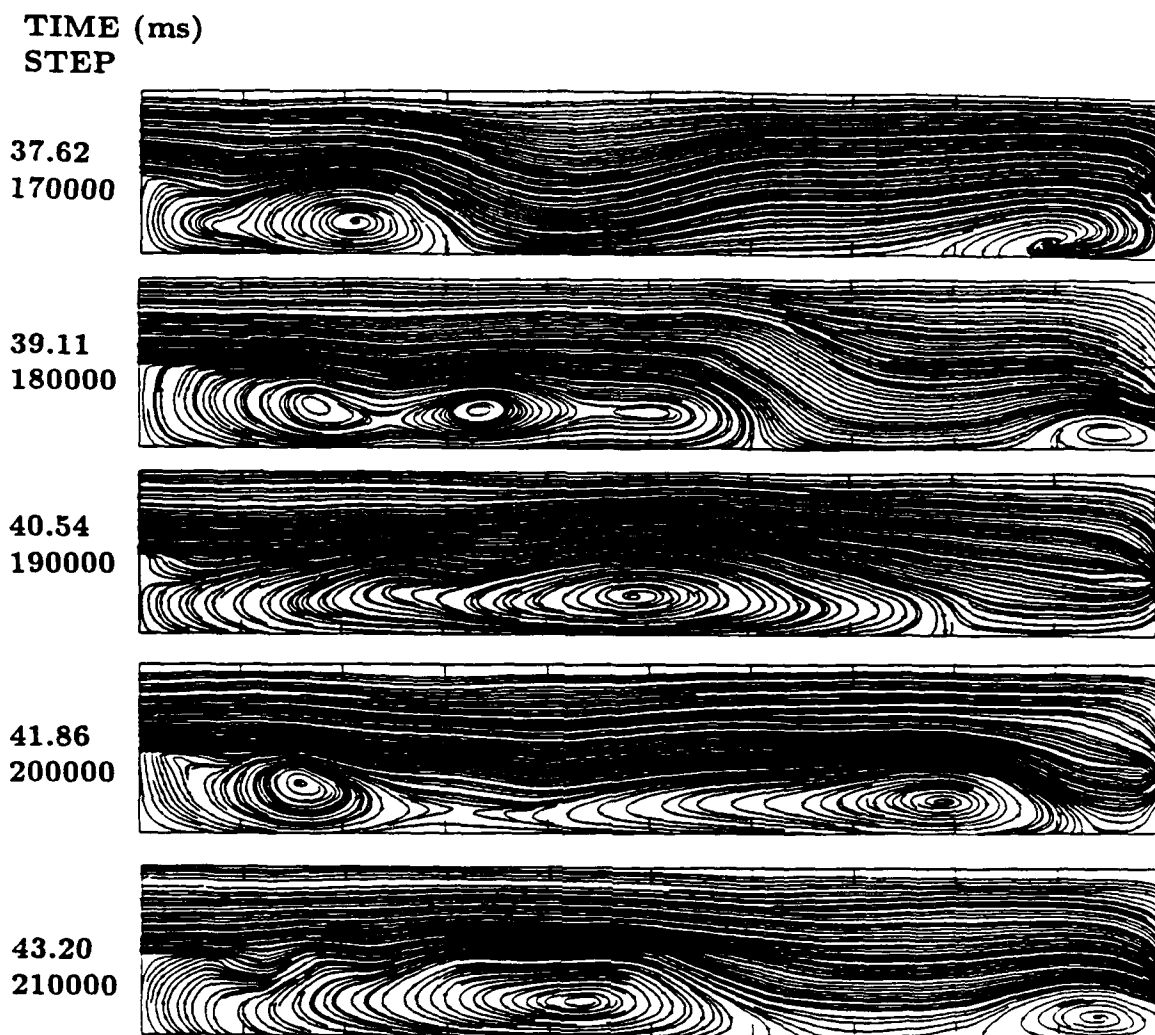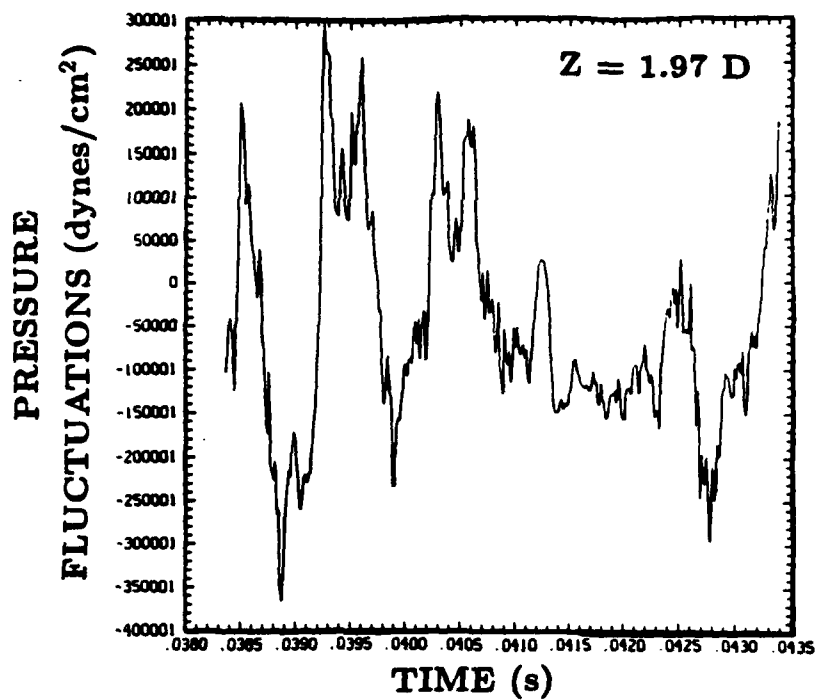
37.62
170000

39.11
180000

40.54
190000

41.86
200000

43.20
210000

Fig. 19 — Streamlines showing the flowfield corresponding to the temperature contours shown in Fig. 18
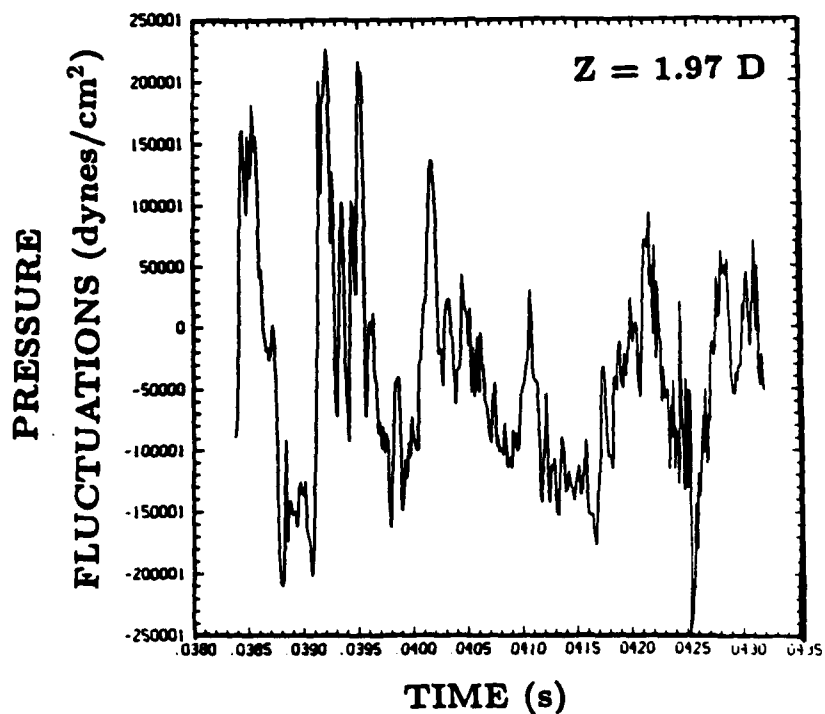
Induction Time Reduced by a Factor of Ten

Fig. 20 — The effect of reducing the induction time on the pressure fluctuations at a particular location in the combustor
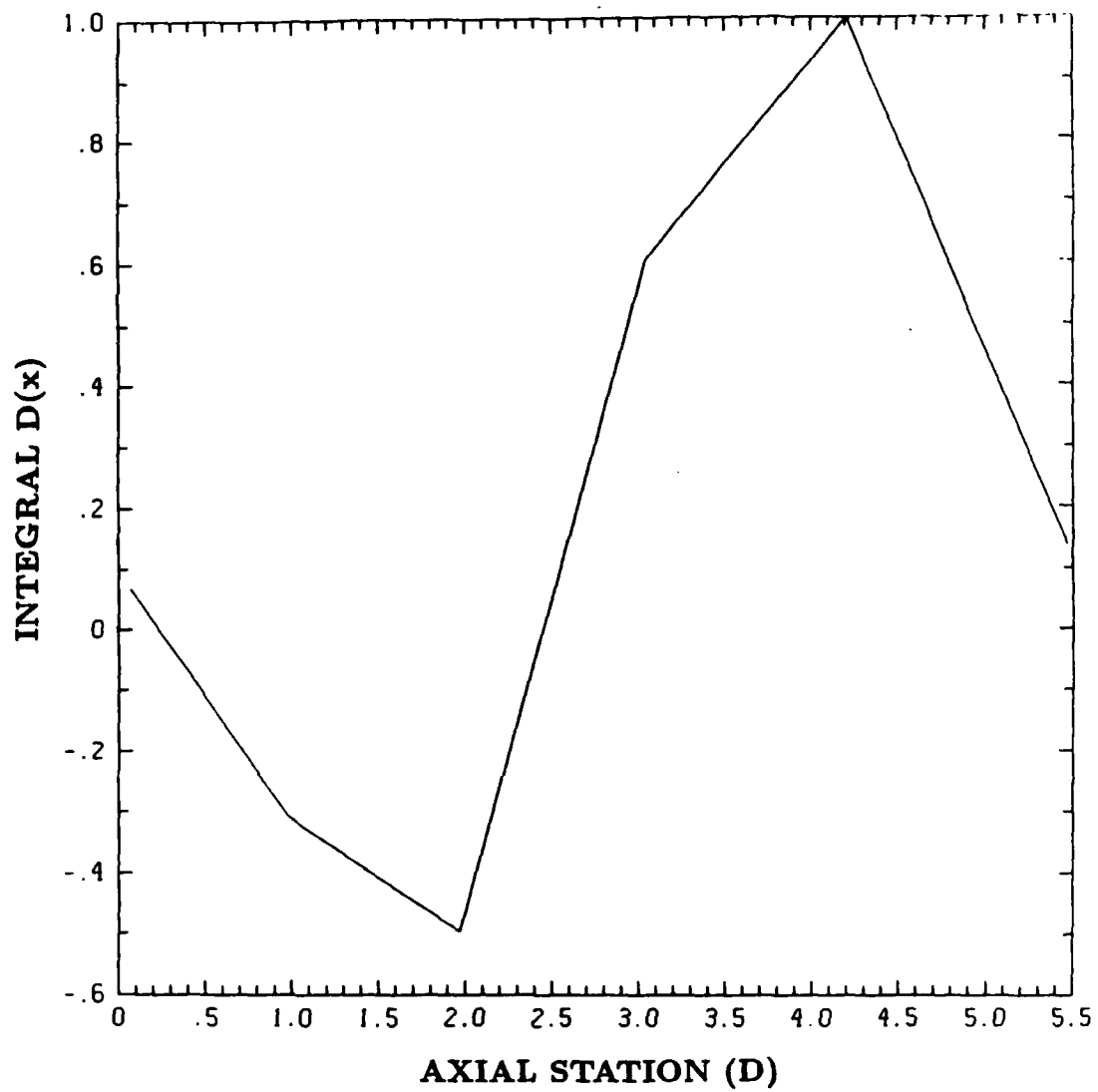
48

Fig. 21 — Time-averaged value of the integral expressing Rayleigh's criterion at a series of axial stations in the combustor for the case in which the induction time is reduced by a factor of ten